

# Transfer matrix and Monte Carlo tests of critical exponents in lattice models

J. Kaupužs \*

Institute of Mathematics and Computer Science, University of Latvia  
29 Rainja Boulevard, LV-1459 Riga, Latvia

February 1, 2008

## Abstract

The corrections to finite-size scaling in the critical two-point correlation function  $G(r)$  of 2D Ising model on a square lattice have been studied numerically by means of exact transfer-matrix algorithms. The systems of square geometry with periodic boundaries oriented either along  $\langle 10 \rangle$  or along  $\langle 11 \rangle$  direction have been considered, including up to 800 spins. The calculation of  $G(r)$  at a distance  $r$  equal to the half of the system size  $L$  shows the existence of an amplitude correction  $\propto L^{-2}$ . A nontrivial correction  $\propto L^{-0.25}$  of a very small magnitude also has been detected in agreement with predictions of our recently developed GFD (grouping of Feynman diagrams) theory. A refined analysis of the recent MC data for 3D Ising,  $\varphi^4$ , and XY lattice models has been performed. It includes an analysis of the partition function zeros of 3D Ising model, an estimation of the correction-to-scaling exponent  $\omega$  from the Binder cumulant data near criticality, as well as a study of the effective critical exponent  $\eta$  and the effective amplitudes in the asymptotic expansion of susceptibility at the critical point. In all cases a refined analysis is consistent with our (GFD) asymptotic values of the critical exponents ( $\nu = 2/3$ ,  $\omega = 1/2$ ,  $\eta = 1/8$  for 3D Ising model and  $\omega = 5/9$  for 3D XY model), while the actually accepted "conventional" exponents are, in fact, effective exponents which are valid for approximation of the finite-size scaling behavior of not too large systems.

**Keywords:** Transfer matrix, Ising model, XY model,  $\varphi^4$  model, critical exponents, finite-size scaling, Monte Carlo simulation

**Pacs:** 64.60.Cn, 68.18.Jk, 05.10.-a

## 1 Introduction

Since the exact solution of two-dimensional Ising model has been found by Onsager [1], a study of various phase transition models is of permanent interest. Nowadays, phase transitions and critical phenomena is one of the most widely investigated fields of physics [2, 3]. Remarkable progress has been reached in exact solution of two-dimensional models [4]. Recently, we have proposed [5] a novel method based on grouping of Feynman diagrams (GFD) in  $\varphi^4$  model. Our GFD theory allows to

---

\*E-mail: kaupuzs@latnet.lv

analyze the asymptotic solution for the two-point correlation function at and near criticality, not cutting the perturbation series. As a result the possible values of exact critical exponents have been obtained [5] for the Ginzburg–Landau ( $\varphi^4$ ) model with  $O(n)$  symmetry, where  $n = 1, 2, 3, \dots$  is the dimensionality of the order parameter. Our predictions completely agree with the known exact and rigorous results in two dimensions [4], and are equally valid also in three dimensions. In [5], we have compared our results to some Monte Carlo (MC) simulations and experiments [6, 7, 8]. It has been shown [5] that the actually discussed MC data for 3D Ising [6] and XY [7] models are fully consistent with our theoretical predictions, but not with those of the perturbative renormalization group (RG) theory [10, 11, 12]. From the theoretical and mathematical point of view, the invalidity of the conventional RG expansions has been demonstrated in [5]. The current paper, dealing with numerical transfer-matrix analysis of the two-point correlation function in 2D Ising model, as well as with the analysis of MC data for the three-dimensional Ising,  $\lambda\varphi^4$  and XY models, presents a more general confirmation that the correct values of critical exponents are those predicted by the GFD theory. Our estimations are based on the finite-size scaling theory, which by itself is an attractive field of investigations [13] and has increasing importance in modern physics [3].

## 2 Critical exponents predicted by GFD theory

Our theory provides possible values of exact critical exponents  $\gamma$  and  $\nu$  for the  $\varphi^4$  model with  $O(n)$  symmetry ( $n$ -component vector model) given by the Hamiltonian

$$H/T = \int \left[ r_0 \varphi^2(\mathbf{x}) + c(\nabla \varphi(\mathbf{x}))^2 + u \varphi^4(\mathbf{x}) \right] d\mathbf{x} , \quad (1)$$

where  $r_0$  is the only parameter depending on temperature  $T$ , and the dependence is linear. At the spatial dimensionality  $d = 2, 3$  and  $n = 1, 2, 3, \dots$  the critical exponents are [5]

$$\gamma = \frac{d + 2j + 4m}{d(1 + m + j) - 2j} , \quad (2)$$

$$\nu = \frac{2(1 + m) + j}{d(1 + m + j) - 2j} , \quad (3)$$

where  $m \geq 1$  and  $j \geq -m$  are integers. At  $n = 1$  we have  $m = 3$  and  $j = 0$  to fit the known exact results for the two-dimensional Ising model. As proposed in Ref. [5], in the case of  $n = 2$  we have  $m = 3$  and  $j = 1$ , which yields in three dimensions  $\nu = 9/13$  and  $\gamma = 17/13$ .

In the present analysis the correction-to-scaling exponent  $\theta$  for the susceptibility is also relevant. The susceptibility is related to the correlation function in the Fourier representation  $G(\mathbf{k})$ , i. e.,  $\chi \propto G(\mathbf{0})$  [11]. In the thermodynamic limit, this relation makes sense at  $T > T_c$ , where  $T_c$  is the critical temperature. According to our theory,  $t^\gamma G(\mathbf{0})$  can be expanded in a Taylor series of  $t^{2\nu-\gamma}$  at  $t \rightarrow 0$ . In this case the reduced temperature  $t$  is defined as  $t = r_0(T) - r_0(T_c) \propto T - T_c$ . Formally,  $t^{2\gamma-d\nu}$  appears as second expansion parameter in the derivations in Ref. [5], but, according to the final result represented by Eqs. (2) and (3),  $(2\gamma - d\nu)/(2\nu - \gamma)$  is a natural

number. Some of the expansion coefficients can be zero, so that in general we have

$$\theta = \ell(2\nu - \gamma), \quad (4)$$

where  $\ell$  may have integer values 1, 2, 3, etc. One can expect that  $\ell = 4$  holds at  $n = 1$  (which yields  $\theta = 1$  at  $d = 2$  and  $\theta = 1/3$  at  $d = 3$ ) and the only nonvanishing corrections are those of the order  $t^\theta$ ,  $t^{2\theta}$ ,  $t^{3\theta}$ , since the known corrections to scaling for physical quantities, such as magnetization or correlation length, are analytical in the case of the two-dimensional Ising model. Here we suppose that the confluent corrections become analytical, i. e.  $\theta$  takes the value 1, at  $d = 2$ . Besides, similar corrections to scaling are expected for susceptibility  $\chi$  and magnetization  $M$  since both these quantities are related to  $G(\mathbf{0})$ , i. e.,  $\chi \propto G(\mathbf{0})$  and  $M^2 = \lim_{x \rightarrow \infty} \langle \varphi(\mathbf{0}) \varphi(\mathbf{x}) \rangle = \lim_{V \rightarrow \infty} G(\mathbf{0})/V$  hold where  $V = L^d$  is the volume and  $L$  is the linear size of the system. The above limit is meaningful at  $L \rightarrow \infty$ , but  $G(\mathbf{0})/V$  may be considered as a definition of  $M^2$  for finite systems too. The latter means that corrections to finite-size scaling for  $\chi$  and  $M$  are similar at  $T = T_c$ . According to the scaling hypothesis and finite-size scaling theory, the same is true for the discussed here corrections at  $t \rightarrow 0$ , where in both cases ( $\chi$  and  $M$ ) the definition  $t = |r_0(T) - r_0(T_c)|$  is valid. Thus, the expected expansion of the susceptibility  $\chi$  looks like  $\chi = t^{-\gamma} (a_0 + a_1 t^\theta + a_2 t^{2\theta} + \dots)$ .

Our hypothesis is that  $j = j(n)$  and  $\ell = \ell(n)$  monotonously increase with  $n$  to fit the known exponents for the spherical model at  $n \rightarrow \infty$ . The analysis of the MC and experimental results here and in [5] enables us to propose that  $j(n) = n - 1$ ,  $\ell(n) = n + 3$ , and  $m = 3$  hold at least at  $n = 1, 2$ . These relations, probably, are true also at  $n \geq 3$ . This general hypothesis is consistent with the idea that the critical exponents  $\gamma$ ,  $\nu$ , and  $\theta$  can be represented by some analytical functions of  $n$  which are valid for all natural positive  $n$  and yield  $\eta = 2 - \gamma/\nu \propto 1/n$  rather than  $\eta \propto 1/n^s$  with  $s = 2, 3, \dots$  ( $s$  must be a natural number to avoid a contradiction, i. e., irrational values of  $j(n)$  at natural  $n$ ) at  $n \rightarrow \infty$ . At these conditions,  $j(n)$  and  $\ell(n)$  are linear functions of  $n$  (with integer coefficients) such that  $\ell(n)/j(n) \rightarrow 1$  at  $n \rightarrow \infty$ , and  $m$  is constant. Besides,  $j(1) = 0$ ,  $m(1) = 3$ , and  $\ell(1) = 4$  hold to coincide with the known results at  $n = 1$ . Then, our specific choice is the best one among few possibilities providing more or less reasonable agreement with the actually discussed numerical and experimental results.

We allow that different  $\ell$  values correspond to the leading correction-to-scaling exponent for different quantities related to  $G(\mathbf{k})$ . The expansion of  $G(\mathbf{k})$  by itself contains a nonvanishing term of order  $t^{2\nu-\gamma} \equiv t^{\eta\nu}$  (in the form  $G(\mathbf{k}) \simeq t^{-\gamma} [g(\mathbf{k}t^{-\nu}) + t^{\eta\nu} g_1(\mathbf{k}t^{-\nu})]$  with  $g_1(\mathbf{0}) = 0$ , since  $\ell > 1$  holds in the case of susceptibility) to compensate the corresponding correction term (produced by  $c(\nabla\varphi)^2$ ) in the equation for  $1/G(\mathbf{k})$  (cf. [5]). The latter means, e. g., that the correlation length  $\xi$  estimated from an approximate ansatz like  $G(\mathbf{k}) \propto 1/[\mathbf{k}^2 + (1/\xi)^2]$  used in [14, 15] also contains a correction proportional to  $t^{\eta\nu}$ . Since  $\eta\nu$  has a rather small value, the presence of such a correction (and, presumably, also the higher order corrections  $t^{2\eta\nu}$ ,  $t^{3\eta\nu}$ , etc.) makes the above ansatz unsuitable for an accurate numerical correction-to-scaling analysis.

The correction  $t^{\eta\nu}$  is related to the correction  $L^{-\eta}$  in the finite-size scaling expressions at criticality. The existence of such a correction in the asymptotic expansion

of the critical real-space Green's (correlation) function is confirmed by our results for the 2D Ising model discussed in Sec. 4.3.

Our consideration can be generalized easily to the case where the Hamiltonian parameter  $r_0$  is a nonlinear analytical function of  $T$ . Nothing is changed in the above expansions if the reduced temperature  $t$ , as before, is defined by  $t = r_0(T) - r_0(T_c)$ . However, analytical corrections to scaling appear (and also corrections like  $(T - T_c)^{m+n\theta}$  with integer  $m$  and  $n$ ) if  $t$  is reexpanded in terms of  $T - T_c$  at  $T > T_c$ . The solution at the critical point remains unchanged, since the phase transition occurs at the same (critical) value of  $r_0$ .

### 3 Exact transfer matrix algorithms for calculation of the correlation function in 2D Ising model

#### 3.1 Adoption of standard methods

The transfer matrix method, applied to analytical calculations on two-dimensional lattices, is well known [1, 4]. However, no analytical methods exist for an exact calculation of the correlation function in 2D Ising model. This can be done numerically by adopting the conventional transfer matrix method and modifying it to reach the maximal result (calculation of as far as possible larger system) with minimal number of arithmetic operations, as discussed further on.

We consider the two-dimensional Ising model where spins are located either on the lattice of dimensions  $N \times L$ , illustrated in Fig. 1a, or on the lattice of dimensions  $\sqrt{2}N \times \sqrt{2}L$ , shown in Fig. 1b. The periodic boundaries are indicated by dashed lines. In case (a) we have  $L$  rows, and in case (b) –  $2L$  rows, each containing  $N$  spins. Fig. 1 shows an illustrative example with  $N = 4$  and  $L = 3$ . Let us  $\sigma(k)$  be the spin variable ( $\pm 1$ ) in the  $k$ -th node of the first row. Here nodes are numbered sequentially from left to right, and rows – from bottom to top. Our method can be used to calculate the correlation (Greens) function between any two spins on the lattice. As an example we consider the Greens function  $G(r)$  in  $\langle 10 \rangle$  crystallographic direction, indicated in Fig. 1 by arrows, i. e.,

$$G(r) = \langle \sigma(k) \sigma(k+r) \rangle \quad : \quad \text{case (a)} \quad (5)$$

$$G(r) = \langle \sigma(k) \sigma'(k + \Delta(r)) \rangle \quad : \quad \text{case (b)} . \quad (6)$$

Here  $\sigma'$  refers to the  $(1+r)$ -th row. It has a shift in the argument  $k$  by  $\Delta(r) = r/2$  for even and  $\Delta(r) = (r-1)/2$  for odd  $r$ . It is supposed that  $\sigma(k+N) \equiv \sigma(k)$  holds according to the periodic boundary conditions.

For convenience, first we consider an application of the transfer matrix method to calculation of the partition function

$$Z = \sum_{\{\sigma_k\}} \exp \left( \beta \sum_{\langle i,j \rangle} \sigma_i \sigma_j \right) , \quad (7)$$

where the summation runs over all the possible spin configurations  $\{\sigma_k\}$ , and the argument of the exponent represents the Hamiltonian of the system including summation over all the neighbouring spin pairs  $\langle i,j \rangle$  of the given configuration  $\{\sigma_k\}$ ;

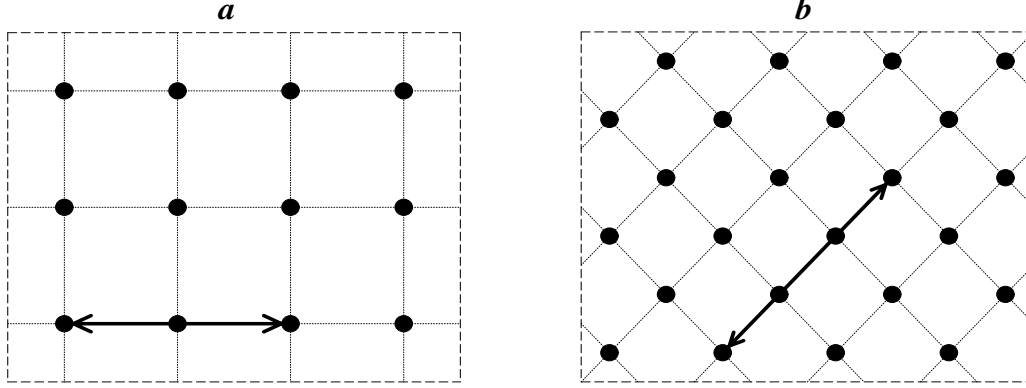


Figure 1: Illustrative examples of the lattices with dimensions  $N \times L$  (a) and  $\sqrt{2}N \times \sqrt{2}L$  (b) with periodic boundary conditions along the dashed lines. The correlation function has been calculated in the  $\langle 10 \rangle$  crystallographic direction, as indicated by the arrows.

parameter  $\beta$  is the coupling constant. Let us consider lattice (a) in Fig. 1, but containing  $n$  rows without periodic boundaries along the vertical axis and without interaction between spins in the upper row. We define the  $2^N$ -component vector  $\mathbf{r}_n$  such that the  $i$ -th component of this vector represents the contribution to the partition function provided by the  $i$ -th spin configuration of the upper row. Then we have an obvious recurrence relation

$$\mathbf{r}_{n+1} = T \mathbf{r}_n , \quad (8)$$

where  $T$  is the transfer matrix with the elements

$$T_{ij} = \exp \left( \beta \sum_k [\sigma(k)]_j [\sigma(k+1)]_j + \beta \sum_k [\sigma(k)]_j [\sigma(k)]_i \right) . \quad (9)$$

Here  $[\sigma(k)]_i$  is the spin variable in the  $k$ -th position in a row provided that the whole set of spin variables of this row forms the  $i$ -th configuration. The first and the second sum in (9) represent the Boltzmann weights for the spin interaction in the  $n$ -th row, and between the  $n$ -th and  $(n+1)$ -th rows, respectively. In this case,  $\mathbf{r}_1$  is the vector with components  $(\mathbf{r}_1)_j = 1$ . If we set

$$(\mathbf{r}_1)_j = \delta_{j,i} , \quad (10)$$

then the components of the resulting vector  $\mathbf{r}_n = \mathbf{r}_n^{(i)}$  give us the partial contributions to the partition function corresponding to a fixed, i. e.  $i$ -th, configuration of the first row. The periodic boundary conditions along the vertical axis means that the  $(L+1)$ -th row must be identical to the first one, i. e., we have to take the  $i$ -th component of the vector  $\mathbf{r}_{L+1}^{(i)}$  and make the summation over  $i$  to get the partition function  $Z$  of the originally defined lattice in Fig. 1a. Note that the missing Boltzmann weights for the interaction between spins in the  $(L+1)$ -th row are already included in the first row. By virtue of (8) and (10), we arrive to the well known expression [4, 16]

$$Z = \sum_i \left( \mathbf{r}_{L+1}^{(i)} \right)_i = \text{Trace} \left( T^L \right) = \sum_i \lambda_i^L , \quad (11)$$

where  $\lambda_i$  are the eigenvalues of the transfer matrix  $T$ . An analogous expression for the lattice in Fig. 1b reads

$$Z = \sum_i \left( \mathbf{r}_{2L+1}^{(i)} \right)_i = \text{Trace} \left( [T_2 T_1]^L \right), \quad (12)$$

where the vectors  $\mathbf{r}_n$  obey the recurrence relation

$$\mathbf{r}_{n+1} = T_{1,2} \mathbf{r}_n \quad (13)$$

similar to (8), but with different transfer matrices  $T_1$  and  $T_2$  for odd and even row numbers  $n$ , respectively. They include the Boltzmann weights for the interaction between two subsequent (odd–even or even–odd, respectively) rows, i. e.,

$$(T_{1,2})_{ij} = \exp \left( \beta \sum_k [\sigma(k)]_i \left\{ [\sigma(k)]_j + [\sigma(k \pm 1)]_j \right\} \right). \quad (14)$$

The actual scheme can be easily adopted to calculate the correlation functions (5) and (6). Namely,  $G(x)$  is given by the statistical average  $Z'/Z$ , where the sum  $Z'$  is calculated in the same way as  $Z$ , but including the corresponding product of spin variables, which implies the following replacements:

$$(\mathbf{r}_1)_j = \delta_{j,i} \Rightarrow (\mathbf{r}_1)_j = \delta_{j,i} \left( N^{-1} \sum_{\ell=1}^N [\sigma(\ell)]_i [\sigma(\ell+x)]_i \right) \quad : \text{case (a)} \quad (15)$$

$$\left( \mathbf{r}_{x+1}^{(i)} \right)_j \Rightarrow \left( \mathbf{r}_{x+1}^{(i)} \right)_j \times \left( N^{-1} \sum_{\ell=1}^N [\sigma(\ell)]_i [\sigma(\ell + \Delta(x))]_j \right) \quad : \text{case (b)}. \quad (16)$$

The index  $i$ , entering in the sums  $Z' = \sum_i \left( \mathbf{r}_{L+1}^{(i)} \right)_i$  [case (a)] and  $Z' = \sum_i \left( \mathbf{r}_{2L+1}^{(i)} \right)_i$  [case (b)], refers to the current configuration of the first row. These equations are obtained by an averaging in (5) and (6) over all the equivalent  $k$  values. Such a symmetrical form allows to reduce the amount of numerical calculations: due to the symmetry we need the summation over only  $\approx 2^N/N$  nonequivalent configurations of the first row instead of the total number of  $2^N$  configurations.

### 3.2 Improved algorithms

The number of the required arithmetic operations can be further reduced if the recurrence relations (8) and (13) are split into  $N$  steps of adding single spin. To formulate this in a suitable way, let us first number all the  $2^N$  spin configurations  $\{\sigma(1); \sigma(2); \dots; \sigma(N-1); \sigma(N)\}$  by an index  $i$  as follows:

$$\begin{aligned} i = 1 & : \{-1; -1; \dots; -1; -1; -1\} \\ i = 2 & : \{-1; -1; \dots; -1; -1; +1\} \\ i = 3 & : \{-1; -1; \dots; -1; +1; -1\} \\ i = 4 & : \{-1; -1; \dots; -1; +1; +1\} \\ & \dots \dots \dots \\ i = 2^N & : \{+1; +1; \dots; +1; +1; +1\} \end{aligned} \quad (17)$$

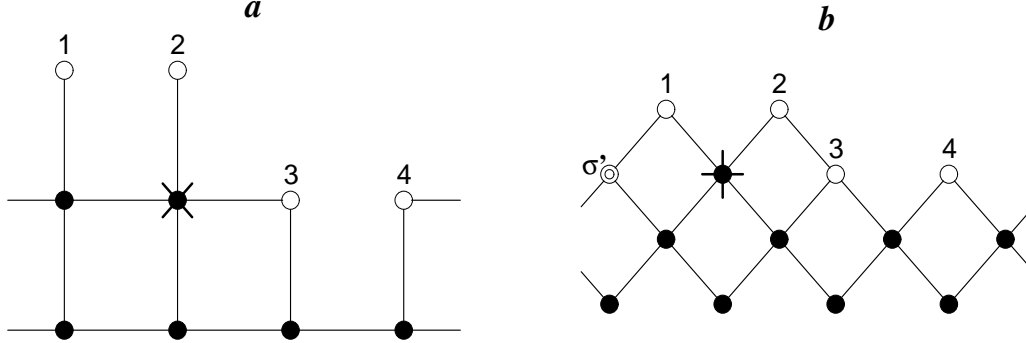


Figure 2: Schematic pictures illustrating the algorithms of calculation for the lattices *a* and *b* introduced in Fig. 1.

We remind that the sequence  $[\sigma(k)]_i$  with  $k = 1, 2, \dots, N$  corresponds to the numbers in the  $i$ -th row. The spin variables in (17) change just like the digits of subsequent integer numbers in the binary counting system.

Consider now a lattice where  $n$  rows are completed, while the  $(n+1)$ -th row contains only  $\ell$  spins where  $\ell < N$ , as illustrated in Fig. 2 in both cases (a) and (b) taking as an example  $N = 4$ . We consider the partial contribution  $(\mathbf{r}_{n+1, \ell})_i$  (i. e.,  $i$ -th component of vector  $\mathbf{r}_{n+1, \ell}$ ) in the partition function  $Z$  (or  $Z'$ ) provided by a fixed ( $i$ -th) configuration of the set of  $N$  upper spins. These are the sequently numbered spins shown in Fig. 2 by empty circles. For simplicity, we have dropped the index denoting the configuration of the first row. In case (b), the spin depicted by a double-circle has a fixed value  $\sigma'$ . In general, this spin is the nearest bottom-left neighbour of the first spin in the upper row. According to this, one has to distinguish between odd and even  $n$ :  $\sigma'$  refers either to the first (for odd  $n$ ), or to the  $N$ -th (for even  $n$ ) spin of the  $n$ -th row. It is supposed that the Boltzmann weights are included corresponding to the solid lines in Fig. 2 connecting the spins. In case (a) the weights responsible for the interaction between the upper numbered spins are not included. Obviously, for a given  $\ell > 1$ ,  $\mathbf{r}_{n+1, \ell}$  can be calculated from  $\mathbf{r}_{n+1, \ell-1}$  via summation over one spin variable, marked in Fig. 2 by a cross. In case (a) it is true also for  $\ell = 1$ , whereas in case (b) this variable has fixed value  $\sigma'$  at  $\ell = 1$ . In the latter case the summation over  $\sigma'$  is performed at the last step when the  $(n+1)$ -th row is already completed. These manipulations enable us to represent the recurrence relation (8) as

$$\mathbf{r}_{n+1} = T \mathbf{r}_n \equiv \widetilde{W}_N \widetilde{W}_{N-1} \cdots \widetilde{W}_2 \widetilde{W}_1 \mathbf{r}_n \quad (18)$$

with

$$\widetilde{W}_\ell = \sum_{\sigma=\pm 1} W_\ell(\sigma), \quad (19)$$

where the componets of the matrices  $W_\ell(\sigma)$  are given by

$$\begin{aligned} (W_1(\sigma))_{ij} &= \delta(j, j_1(\sigma, 1, i)) \cdot \exp(\beta \sigma \{[\sigma(1)]_i + [\sigma(2)]_i + [\sigma(N)]_i\}) \\ (W_\ell(\sigma))_{ij} &= \delta(j, j_1(\sigma, \ell, i)) \cdot \exp(\beta \sigma \{[\sigma(\ell)]_i + [\sigma(\ell+1)]_i\}) : 1 < \ell < N \\ (W_N(\sigma))_{ij} &= \delta(j, j_1(\sigma, N, i)) \cdot \exp(\beta \sigma [\sigma(N)]_i). \end{aligned} \quad (20)$$

Here  $\delta(j, k)$  is the Kronecker symbol and

$$j_1(\sigma, \ell, i) = i + (\sigma - [\sigma(\ell)]_i) 2^{N-\ell-1} \quad (21)$$

are the indexes of the old configurations containing  $\ell - 1$  spins in the  $(n + 1)$ -th row depending on the value  $\sigma$  of the spin marked in Fig. 2a by a cross, as well as on the index  $i$  of the new configuration with  $\ell$  spins in the  $(n + 1)$ -th row, as consistent with the numbering (17).

The above equations (18) to (20) refers to case (a). In case (b) we have

$$\mathbf{r}_{n+1} = T_{1,2} \mathbf{r}_n \equiv \sum_{\sigma'=\pm 1} \widetilde{W}_N^{(1,2)} \widetilde{W}_{N-1}^{(1,2)} \dots \widetilde{W}_2^{(1,2)} W_1^{(1,2)}(\sigma') \mathbf{r}_n, \quad (22)$$

where  $\widetilde{W}_\ell^{(1,2)}$  are the matrices

$$\widetilde{W}_\ell^{(1,2)} = \sum_{\sigma=\pm 1} W_\ell^{(1,2)}(\sigma). \quad (23)$$

Here indexes 1 and 2 refer to odd and even row numbers  $n$ , respectively, and the components of the matrices  $W_\ell^{(1,2)}(\sigma)$  are

$$\left( W_\ell^{(1,2)}(\sigma) \right)_{ij} = \delta(j, j_{1,2}(\sigma, \ell, i)) \cdot \exp(\beta [\sigma(\ell)]_i \{ \sigma + [\sigma(\ell + 1)]_i \}) , \quad (24)$$

where  $[\sigma(N + 1)]_i \equiv \sigma'$  and the index  $j_1(\sigma, \ell, i)$  is given by (21). For the other index we have

$$\begin{aligned} j_2(\sigma, 1, i) &= 2i - 2^{N-1} ([\sigma(1)]_i + 1) + \frac{1}{2}(\sigma - 1) \\ j_2(\sigma, \ell, i) &= j_1(\sigma, \ell, i) \quad : \quad \ell \geq 2. \end{aligned} \quad (25)$$

Note that the matrices  $\widetilde{W}_\ell$  and  $\widetilde{W}_\ell^{(1,2)}$  have only two nonzero elements in each row, so that the number of the arithmetic operations required for the construction of one row of spins via subsequent calculation of the vectors  $\mathbf{r}_{n+1, \ell}$  increases like  $2N \cdot 2^N$  instead of  $2^{2N}$  operations necessary for a straightforward calculation of the vector  $T\mathbf{r}_n$ . Taking into account the above discussed symmetry of the first row, the computation time is proportional to  $2^{2L}L$  for both  $L \times L$  (a) and  $\sqrt{2}L \times \sqrt{2}L$  (b) lattices in Fig. 1 with periodic boundary conditions.

### 3.3 Application to different boundary conditions

The developed algorithms can be easily extended to the lattices with antiperiodic boundary conditions. The latter implies that  $\sigma(N + 1) = -\sigma(N)$  holds for each row, and similar condition is true for each column. We can consider also the mixed boundary conditions: periodic along the horizontal axis and antiperiodic along the vertical one, or vice versa. To replace the periodic boundary conditions with the antiperiodic ones we need only to change the sign of the corresponding products of the spin variables on the boundaries. Consider, e. g., the case (a) in Fig. 1. The change of the boundary conditions along the vertical axis means that the first term in the argument of the exponent in each of the Eqs. (20) changes the sign for the last row, i. e., when  $n = L$ . The same along the horizontal axis implies that the term  $[\sigma(N)]_i$  in the equation for  $(W_1(\sigma))_{ij}$  changes the sign. In this case, however, the symmetry with respect to the configurations of the first row is partly broken and, therefore, we need summation over a larger number of nonequivalent configurations.



## 4 Transfer matrix study of critical Greens function and corrections to scaling in 2D Ising model

### 4.1 General scaling arguments

It is well known that in the thermodynamic limit the real-space Greens function of the Ising model behaves like  $G(r) \propto r^{2-d-\eta}$  at large distances  $r \rightarrow \infty$  at the critical point  $\beta = \beta_c$ , where  $\eta$  is the critical exponent having the value  $\eta = 1/4$  in two dimensions ( $d = 2$ ). Based on our transfer matrix algorithms developed in Sec 3, here we test the finite-size scaling and, particularly, the corrections to scaling at criticality.

In [5] the critical correlation function in the Fourier representation, i. e.  $G(\mathbf{k})$  at  $T = T_c$ , has been considered for the  $\varphi^4$  model. In this case the minimal value of the wave vector magnitude  $k$  is related to the linear system size  $L$  via  $k_{min} = 2\pi/L$ . In analogy to the consideration in Sec. 5.2 of [5], one expects that  $k/k_{min}$  is an essential finite-size scaling argument, corresponding to  $r/L$  in the real space. In the Ising model at  $r \sim L$  one has to take into account also the anisotropy effects, so that the expected finite-size scaling relation for the real-space Greens function at the critical point  $\beta = \beta_c$  reads

$$G(r) \simeq r^{2-d-\eta} f(r/L) \quad : \quad r \rightarrow \infty, L \rightarrow \infty, \quad (26)$$

where the scaling function  $f(z)$  depends also on the crystallographic orientation of the line connecting the correlating spins, as well as on the orientation of the periodic boundaries. A natural extension of (26), including the corrections to scaling, is

$$G(r) = \sum_{\ell \geq 0} r^{-\lambda_\ell} f_\ell(r/L), \quad (27)$$

where the term with  $\lambda_0 \equiv d - 2 + \eta$  is the leading one, whereas those with the subsequently increasing exponents  $\lambda_1, \lambda_2$ , etc., represent the corrections to scaling. By a substitution  $f_\ell(z) = z^{\lambda_\ell} \tilde{f}_\ell(z)$ , the asymptotic expansion (27) transforms to

$$G(r) = f'_0(r/L) L^{-\lambda_0} \left( 1 + \sum_{\ell \geq 1} L^{-\omega_\ell} \tilde{f}_\ell(r/L) \right), \quad (28)$$

where  $\tilde{f}_\ell(z) = f'_\ell(z)/f'_0(z)$  and  $\omega_\ell = \lambda_\ell - \lambda_0$  are the correction-to-scaling exponents.

We have tested the scaling relation (26) in 2D Ising model by using the exact transfer matrix algorithms in Sec. 3. Consider, e. g., the correlation function in  $\langle 10 \rangle$  crystallographic direction in the specific case (a) discussed in Sec. 3. According to (26), all points of  $f(r/L) = r^{1/4} G(r)$  corresponding to large enough values of  $r$  and  $L$  should well fit a common smooth line, as it is actually observed in Fig 3 at  $2 \leq r \leq L/2$  and  $L = 8, 12, 15$ , and 18. This example shows that the corrections to (26) are rather small, since the deviations from the spline curve constructed at  $L = 18$  are very small at relatively small  $L$  values and even at  $r = 2$ . In general, our calculations provide a strong numerical evidence of correctness of the asymptotic expansion (28): at a given ratio  $r/L$ , the correlation function is described by an expansion in  $L$  powers with a really striking accuracy. Namely, our numerical analysis, which is sensitive to a variation of  $G(r)$  in the fourteens digit, does not reveal an inconsistency with this asymptotic expansion.

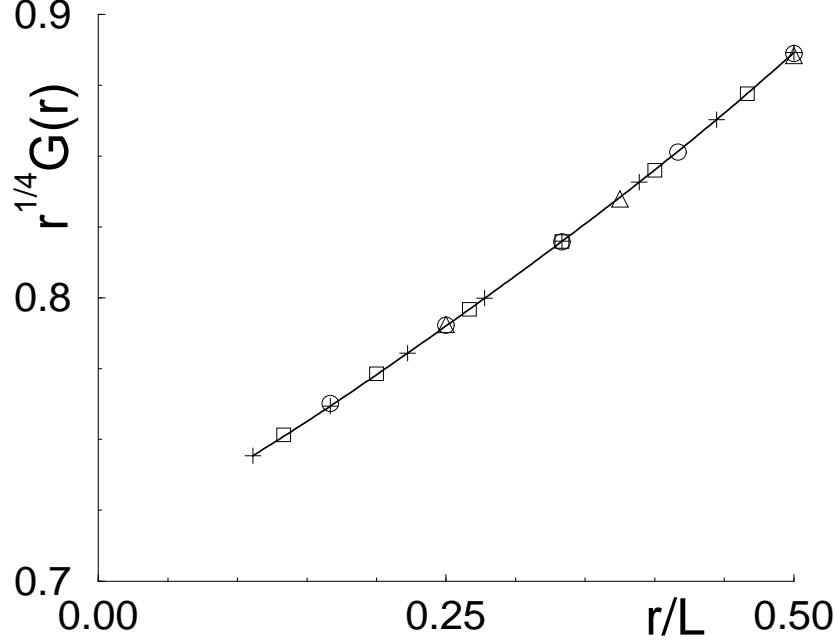


Figure 3: Test of the finite-size scaling relation  $G(r) \simeq r^{-1/4} f(r/L)$  in 2D Ising model on a square  $L \times L$  lattice with periodic boundary conditions. The values of the scaling function  $f(r/L)$  estimated at  $L = 8$  (triangles),  $L = 12$  (circles),  $L = 15$  (squares), and  $L = 18$  (pluses) well lie on a common smooth line showing that corrections to this scaling relation are small.

## 4.2 Correction-to-scaling analysis for the $L \times L$ lattice

Based on the scaling analysis in Sec. 4.1, here we discuss the corrections to scaling for the lattice in Fig. 1a. We have calculated the correlation function  $G(r)$  at a fixed ratio  $r/L = 0.5$  in  $\langle 10 \rangle$  direction, as well as at  $r/L = 0.5\sqrt{2}$  in  $\langle 11 \rangle$  direction at  $L = 2, 4, 6, \dots$  with an aim to identify the correction exponents in (28). Note that in the latter case the replacement (16) is valid for  $G(\sqrt{2}x)$  (where  $x = 1, 2, 3, \dots$ ) with the only difference that  $\Delta(x) = x$ .

Let us define the effective correction-to-scaling exponent  $\omega_{eff}(L)$  in 2D Ising model via the solution of the equations

$$\tilde{L}^{1/4} G(r = \text{const} \cdot \tilde{L}) = a + b \tilde{L}^{-\omega_{eff}} \quad (29)$$

at  $\tilde{L} = L, L + \Delta L, L + 2\Delta L$  with respect to three unknown quantities  $\omega_{eff}$ ,  $a$ , and  $b$ . According to (28), where  $\lambda_0 = \eta = 1/4$ , such a definition gives us the leading correction-to-scaling exponent  $\omega$  at  $L \rightarrow \infty$ , i. e.,  $\lim_{L \rightarrow \infty} \omega_{eff}(L) = \omega$ .

The calculated values of  $G(r = c \cdot L)$  in the  $\langle 10 \rangle$  and  $\langle 11 \rangle$  crystallographic directions [in case (a)] with  $c = 0.5$  and  $c = 0.5\sqrt{2}$ , respectively, and the corresponding effective exponents  $\omega_{eff}(L)$ , determined at  $\Delta L = 2$ , are given in Tab. 1. In both cases the effective exponent  $\omega_{eff}(L)$  seems to converge to a value about 2. Besides, in the second case the behavior is more smooth, so that we can try somehow to extrapolate the obtained sequence of  $\omega_{eff}$  values (column 5 in Tab. 1) to  $L = \infty$ .

Table 1: The correlation function  $G(r = c \cdot L)$  in  $\langle 10 \rangle$  ( $c = 0.5$ ) and  $\langle 11 \rangle$  ( $c = 0.5\sqrt{2}$ ) crystallographic directions vs the linear size  $L$  of the lattice (a) in Fig. 1, and the corresponding effective exponents  $\omega_{eff}(L)$  and  $\tilde{\omega}(L)$ .

L	direction $\langle 10 \rangle$		direction $\langle 11 \rangle$		
	$G(0.5L)$	$\omega_{eff}(L)$	$G(0.5\sqrt{2}L)$	$\omega_{eff}(L)$	$\tilde{\omega}(L)$
2	0.84852813742386	2.7366493	0.8	1.8672201	
4	0.74052044609665	2.9569864	0.71375464684015	2.2148707	
6	0.67202206468538	1.8998036	0.65238484475089	2.1252078	
8	0.62605120856389	1.5758895	0.60935351016910	2.0611362	1.909677
10	0.59238112628953	1.6617494	0.57724041054810	2.0351831	1.996735
12	0.56615525751968	1.7774398	0.55200680271678	2.0232909	2.002356
14	0.54485584658226	1.8542943	0.53141907668442	2.0167606	2.001630
16	0.52703456475995		0.51414720882560		
18	0.51178753041103		0.49934511003360		

For this purpose we have considered the ratio of two subsequent increments in  $\omega_{eff}$ ,

$$r(L) = \frac{\omega_{eff}(L + \Delta L) - \omega_{eff}(L)}{\omega_{eff}(L) - \omega_{eff}(L - \Delta L)}. \quad (30)$$

A simple analysis shows that  $r(L)$  behaves like

$$r(L) = 1 - \Delta L \cdot (\omega' + 1)L^{-1} + o(L^{-2}) \quad (31)$$

at  $L \rightarrow \infty$  if  $\omega_{eff}(L) = \omega + o(L^{-\omega'})$  holds with an exponent  $\omega' > 1$ . The numerical data in Tab. 1 show that Eq. (31) represents a good approximation for the largest values of  $L$  at  $\omega' = 2$ . It suggests us that the leading and the subleading correction exponents in (28) could be  $\omega \equiv \omega_1 = 2$  and  $\omega_2 = 4$ , respectively. Note that  $\omega_{eff}(L)$  can be defined with a shift in the argument. Our specific choice ensures the best approximation by (31) at the actual finite  $L$  values.

Let us now assume that the values of  $\omega_{eff}(L)$  are known up to  $L = L_{max}$ . Then we can calculate from (30) the  $r(L)$  values up to  $L = L_{max} - \Delta L$  and make a suitable ansatz like

$$r(L) = 1 - 3\Delta L \cdot L^{-1} + bL^{-2} \quad \text{at } L \geq L_{max} \quad (32)$$

for a formal extrapolation of  $\omega_{eff}(L)$  to  $L = \infty$ . This is consistent with (31) where  $\omega' = 2$ . The coefficient  $b$  is found by matching the result to the precisely calculated value at  $L = L_{max} - \Delta L$ . The subsequent values of  $\omega_{eff}(L)$ , calculated from (30) and (32) at  $L > L_{max}$ , converge to some value  $\tilde{\omega}(L_{max})$  at  $L \rightarrow \infty$ . If the leading correction-to-scaling exponent  $\omega$  is 2, indeed, then the extrapolation result  $\tilde{\omega}(L_{max})$  will tend to 2 at  $L_{max} \rightarrow \infty$  irrespective to the precise value of  $\omega'$ .

As we see from Tab. 1, the values of  $\tilde{\omega}(L)$  come remarkably closer to 2 as compared to  $\omega_{eff}(L)$ , which seems to indicate that  $\omega = 2$ . However, as we have discussed in Sec. 2, there should be a nontrivial correction in (28) with  $\omega = \eta = 1/4$ . The

Table 2: The correlation function  $G(r = L)$  in  $\langle 10 \rangle$  crystallographic direction and the effective exponents  $\omega_{eff}(L)$  and  $\tilde{\omega}(L)$  vs the linear size  $L$  of the lattice (b) in Fig. 1.

L	$G(L)$	$\omega_{eff}(L)$	$\tilde{\omega}(L)$
2	0.8		
3	0.7203484812087670		
4	0.6690636562097066		
5	0.6321925914229602		
6	0.6037455936471098		
7	0.5807668304926868		
8	0.5616046762441826	2.066235298	
9	0.5452468033693456	2.043461090	
10	0.5310294874153481	2.030235674	1.996772124
11	0.5184950262041604	2.022130104	1.999333324
12	0.5073151480587211	2.016864947	1.999941357
13	0.4972468711401118	2.013265826	2.000036957
14	0.4881056192765374	2.010701166	2.000040498
15	0.4797481011874659	2.008811505	2.000044005
16	0.4720609977942179	2.007380630	2.000053415
17	0.4649532511721054	2.006272191	2.000063984
18	0.4583506666254706	2.005396785	2.000073711
19	0.4521920457268738		
20	0.4464263594840965		

fact that this nontrivial correction does not manifest itself in the above numerical analysis can be understood assuming that this correction term has a very small amplitude.

### 4.3 Correction-to-scaling analysis for the $\sqrt{2}L \times \sqrt{2}L$ lattice

To test the existence of nontrivial corrections to scaling, as proposed at the end of Sec. 4.2, here we make the analysis of the correlation function  $G(r)$  in  $\langle 10 \rangle$  direction on the  $\sqrt{2}L \times \sqrt{2}L$  lattice shown in Fig. 1b. The advantage of case (b) in Fig. 1 as compared to case (a) is that  $\sqrt{2}$  times larger lattice corresponds to the same number of the spins in one row. Besides, in this case we can use not only even, but all lattice sizes to evaluate the exponent  $\omega$  from calculations of  $G(r = L)$ , which means that it is reasonable to use the step  $\Delta L = 1$  to evaluate  $\omega_{eff}$  and  $\tilde{\omega}(L)$  from Eqs. (29), (30) and (32). The results, are given in Tab. 2.

It is evident from Tab. 2 that the extrapolated values of the effective correction exponent, i. e.  $\tilde{\omega}(L)$ , come surprisingly close to 2 at certain  $L$  values. Besides, the ratio of increments  $r$  [cf. Eq. (30)] in this case is well approximated by (32), as consistent with existence of a correction term in (28) with exponent 4. On the other hand, we can see from Tab. 2 that  $\Delta\tilde{\omega}(L) = \tilde{\omega}(L) - 2$  tends to increase in magnitude at  $L > 13$ . We have illustrated this systematic and smooth deviation in Fig. 4. The only reasonable explanation of this behavior is that the expansion (28) necessarily

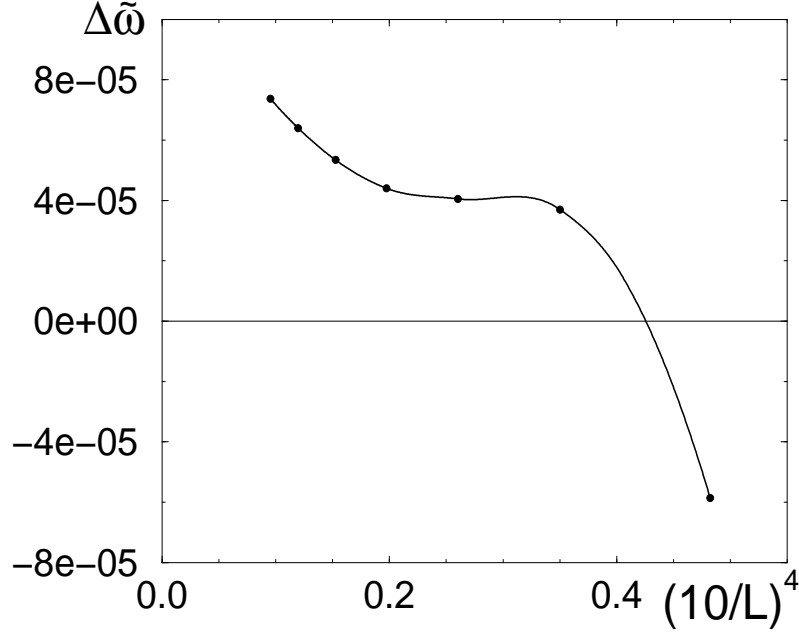


Figure 4: The deviation of the extrapolated effective exponent  $\Delta\tilde{\omega}(L) = \tilde{\omega}(L) - 2$  as a function of  $L^{-4}$ . The extrapolation has been made by using the calculated  $G(r)$  values in Tab. 2 up to the size  $L + 2$ . A linear convergence to zero would be expected in absence of any correction term with exponent  $\omega < 2$ .

contains the exponent 2 and, likely, also the exponent 4, and at the same time it contains also a correction of a very small amplitude with  $\omega < 2$ . The latter explains the increase of  $\Delta\tilde{\omega}(L)$ . Namely, the correction to scaling for  $L^{1/4}G(L)$  behaves like  $const \cdot L^{-2} [1 + o(L^{-2}) + \varepsilon L^{2-\omega}]$  with  $\varepsilon \ll 1$ , which implies a slow crossover of the effective exponent  $\omega_{eff}(L)$  from the values about 2 to the asymptotic value  $\omega$ . Besides, in the region where  $\varepsilon L^{2-\omega} \ll 1$  holds, the effective exponent behaves like

$$\omega_{eff}(L) \simeq 2 + b_1 L^{2-\omega} + b_2 L^{-2}, \quad (33)$$

where  $b_1 \ll 1$  and  $b_2$  are constants. By using the extrapolation of  $\omega_{eff}$  with  $\omega' = 2$  in (31) and (32), we have compensated the effect of the correction term  $b_2 L^{-2}$ . Besides, by matching the amplitude  $b$  in (32) we have compensated also the next trivial correction term  $\sim L^{-3}$  in the expansion of  $\omega_{eff}(L)$ . It means that the extrapolated exponent  $\tilde{\omega}(L)$  does not contain these expansion terms, i. e., we have

$$\tilde{\omega}(L) = 2 + b_1 L^{2-\omega} + \delta\tilde{\omega}(L), \quad (34)$$

where  $\delta\tilde{\omega}(L)$  represents a remainder term. It includes the trivial corrections like  $L^{-4}$ ,  $L^{-5}$ , etc., and also subleading nontrivial corrections, as well as corrections of order  $(\varepsilon L^{2-\omega})^2$ ,  $(\varepsilon L^{2-\omega})^3$ , etc., neglected in (33). According to the latter, Eq. (34) is meaningless in the thermodynamic limit  $L \rightarrow \infty$ , but it can be used to evaluate the correction-to-scaling exponent  $\omega$  from the transient behavior at large, but not too large values of  $L$  where  $b_1 L^{2-\omega} \ll 1$  holds. In our example the latter condition is well satisfied, indeed.

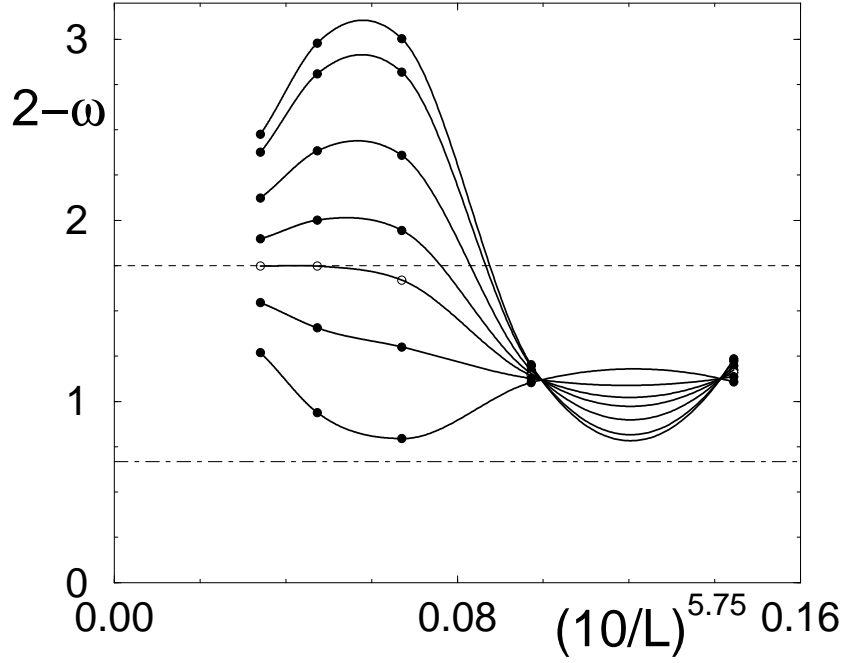


Figure 5: The exponent  $2 - \omega$  estimated from (37) at different system sizes. From top to bottom (if looking on the left hand side):  $\alpha = 0, 1, 3.5, 5.75, 7.243, 9.25, 12$ . The results at the optimal  $\alpha$  value 7.243 are shown by empty circles. The dashed line indicates our theoretical asymptotic value  $2 - \omega = 1.75$ , whereas the dot-dashed line – that proposed in [17].

Based on (34), we have estimated the nontrivial correction-to-scaling exponent  $\omega$  by using the data of  $\tilde{\omega}(L)$  in Tab 2. We have used two different ansatzs

$$2 - \omega_1(L) = \ln [\Delta\tilde{\omega}(L)/\Delta\tilde{\omega}(L-1)] / \ln[L/(L-1)] \quad (35)$$

and

$$2 - \omega_2(L) = L [\Delta\tilde{\omega}(L) - \Delta\tilde{\omega}(L-1)] / \Delta\tilde{\omega}(L) , \quad (36)$$

as well as the linear combination of them

$$\omega(L) = (1 - \alpha) \omega_1(L) + \alpha \omega_2(L) \quad (37)$$

containing a free parameter  $\alpha$ . We have  $\omega(L) = \omega_1(L)$  at  $\alpha = 0$  and  $\omega(L) = \omega_2(L)$  at  $\alpha = 1$ . In general, the effective exponent  $\omega(L)$  converges to the same result  $\omega$  at arbitrary value of  $\alpha$ , but at some values the convergence is better. The results for  $2 - \omega(L)$  vs  $L^{\omega-6}$  at different  $\alpha$  values are represented in Fig. 5 by a set of curves. In this scale the convergence to the asymptotic value would be linear (within the actual region where  $L \gg 1$  and  $b_1 L^{2-\omega} \ll 1$  hold) for  $\alpha = 0$  at the condition  $\delta\tilde{\omega}(L) \propto L^{-4}$ . We have chosen the scale of  $L^{-5.75}$ , as it is consistent with our theoretical prediction in Sec. 2 that  $\omega = 1/4$ . Nothing is changed essentially if we use slightly different scale as, e. g.,  $L^{-14/3}$  consistent with the correction-to-scaling exponent  $\omega = 4/3$  proposed in [17]. As we see from Fig. 5, all curves tend to merge at our asymptotic value  $2 - \omega = 1.75$  shown by a dashed line. The optimal value of  $\alpha$  is defined by the condition that the last two estimates  $\omega(17)$  and  $\omega(18)$  agree with each other. It occurs at  $\alpha = 7.243$ , and the last two points lie just on our theoretical line.

It is interesting to compare our results with those of the high temperature (HT) series analysis in [18]. The authors of [18] have found “almost by inspection” a correction with exponent  $\omega = 9/4$  in the asymptotic expansion of the susceptibility  $\chi$ . If such a correction exists in the susceptibility, it must be present also in the correlation function due to the relation  $\chi = \sum_{\mathbf{x}} G(\mathbf{x}_1 - \mathbf{x})$ . Surprisingly, our extremely accurate calculations by exact algorithms have not revealed such a correction. Our analysis shows that nontrivial corrections exist, indeed, in the correlation function of 2D Ising model, but they are so extremely small and strongly masked by trivial corrections like  $L^{-2}$  and  $L^{-4}$  that they could not be detected by approximate methods like HT series expansion.

#### 4.4 Comparison to the known exact results and estimation of numerical errors

We have carefully checked our algorithms comparing the results with those obtained via a straightforward counting of all spin configurations for small lattices, as well as comparing the obtained values of the partition function to those calculated from the known exact analytical expressions. Namely, an exact expression for the partition function of a finite-size 2D lattice on a torus with arbitrary coupling constants between each pair of neighbouring spins has been reported in [19] obtained by the loop counting method and represented by determinants of certain transfer matrices. In the standard 2D Ising model with only one common coupling constant  $\beta$  these matrices can be diagonalized easily, using the standard techniques [20]. Besides, the loop counting method can be trivially extended to the cases with antiperiodic or mixed boundary conditions discussed in Sec. 3.3. It is necessary only to mention that each loop gets an additional factor  $-1$  when it winds round the torus with antiperiodic boundary conditions. We consider the partition functions  $Z_{pp} \equiv Z$ ,  $Z_{aa}$ ,  $Z_{ap}$ ,  $Z_{pa}$ . In this notation the first index refers to the horizontal or  $x$  axis, and the second one – to the vertical or  $y$  axis of a lattice illustrated in Fig. 1a;  $p$  means periodic and  $a$  – antiperiodic boundary conditions. As explained above, the standard methods leads to the following exact expressions:

$$\begin{aligned} Z_{pp} &= (Q_1 + Q_2 + Q_3 - Q_0) / 2 \\ Z_{ap} &= (Q_0 + Q_1 + Q_3 - Q_2) / 2 \\ Z_{pa} &= (Q_0 + Q_1 + Q_2 - Q_3) / 2 \\ Z_{aa} &= (Q_0 + Q_2 + Q_3 - Q_1) / 2 \end{aligned} \tag{38}$$

where  $Q_0$  is the partition function represented by the sum of the closed loops on the lattice, as consistent with the loop counting method in [20], whereas  $Q_1$ ,  $Q_2$ , and  $Q_3$  are modified sums with additional factors  $\exp(\Delta x \cdot i\pi/N + \Delta y \cdot i\pi/L)$ ,  $\exp(\Delta x \cdot i\pi/N)$ , and  $\exp(\Delta y \cdot i\pi/L)$ , respectively, related to each change of coordinate  $x$  by  $\Delta x = \pm 1$ , or coordinate  $y$  by  $\Delta y = \pm 1$  when making a loop. The standard manipulations [20] yield

$$\begin{aligned} Q_i &= 2^{NL} \prod_{q_x, q_y} \left[ \cosh^2(2\beta) - \sinh(2\beta) \right. \\ &\quad \times \left( \cos \left[ q_x + (\delta_{i,1} + \delta_{i,2}) \frac{\pi}{N} \right] + \cos \left[ q_y + (\delta_{i,1} + \delta_{i,3}) \frac{\pi}{L} \right] \right) \Big]^{1/2}, \end{aligned} \tag{39}$$

where the wave vectors  $q_x = (2\pi/N) \cdot n$  and  $q_y = (2\pi/L) \cdot \ell$  run over all the values corresponding to  $n = 0, 1, 2, \dots, N-1$  and  $\ell = 0, 1, 2, \dots, L-1$ . In the case of the periodic boundary conditions, each loop of  $Q_0$  has the sign  $(-1)^{m+ab+a+b}$  [19], where  $m$  is the number of intersections,  $a$  is the number of windings around the torus in  $x$  direction, and  $b$  – in  $y$  direction. The correct result for  $Z_{pp}$  is obtained if each of the loops has the sign  $(-1)^m$ . In all other cases, similar relations are found easily, taking into account the above defined additional factors. Eqs. (38) are then obtained by finding such a linear combination of quantities  $Q_i$  which ensures the correct weight for each kind of loops.

All our tests provided a perfect agreement between the obtained values of the Greens functions  $G(r)$  (a comparison between straightforward calculations and our algorithms), as well as between partition functions for different boundary conditions (a comparison between our algorithms and Eq. (38)). The relative discrepancies were extremely small (e. g.,  $10^{-15}$ ), obviously, due to the purely numerical inaccuracy.

We have used the double-precision FORTRAN programs. The main source of the inaccuracy in our calculations is the accumulation of numerical errors during the summation of long sequences of numbers, i. e., during the summation over all the nonequivalent configurations of the first row of spins. To eliminate the error for the largest lattice  $L = 20$ , we have split the summation in several parts in such a way that a relatively small part, including only the first 10 000 configurations from the total number of 52 487 nonequivalent ones, gives the main contribution to  $Z$  and  $Z'$ . The same trick with splitting in two approximately equal parts has been used at  $L = 19$ , as well. By comparing the summation results with different splittings, we have concluded that a systematical error in  $G(r)$  at  $L = 20$  could reach the value about  $3 \cdot 10^{-15}$ . The calculations at  $L = 18$  and  $19$  have been performed with approximately the same accuracy. The systematical errors in subsequent  $G(r)$  values tend to compensate in the final result for  $\omega(L)$ . The resulting numerical errors in Fig. 5 are about 0.02 or 0.03, i. e., approximately within the symbol size.

## 5 Analysis of the partition function zeros in 3D Ising model

In this section we discuss the recent MC results [9] for the complex zeros of the partition function of the three-dimensional Ising model. Namely, if the coupling  $\beta$  is a complex number, then the partition sum has zeros at certain complex values of  $\beta$  or  $u = e^{-\beta}$ . The nearest to the real positive axis values  $\beta_1^0$  and  $u_1^0$  are of special interest. Neglecting the second-order corrections,  $u_1^0$  behaves like

$$u_1^0 = u_c + A L^{-1/\nu} + B L^{-(1/\nu)-\omega} \quad (40)$$

at large  $L$ , where  $u_c = e^{-\beta_c}$  is the critical value of  $u$ ,  $A$  and  $B$  are complex constants, and  $\omega$  is the correction-to-scaling exponent. According to the known solution given in [20, 21], the partition function zeros correspond to complex values of  $\sinh(2\beta)$  located on a unit circle in the case of 2D Ising model, so that  $A$  is purely imaginary. This solution, however, is only asymptotically exact at  $L \rightarrow \infty$ . Nevertheless, based on an analysis of the exact expression Eq. (38) we conclude that the statement  $\text{Re } A = 0$  is correct. This fact is obvious in the case of Brascamp-Kunz boundary



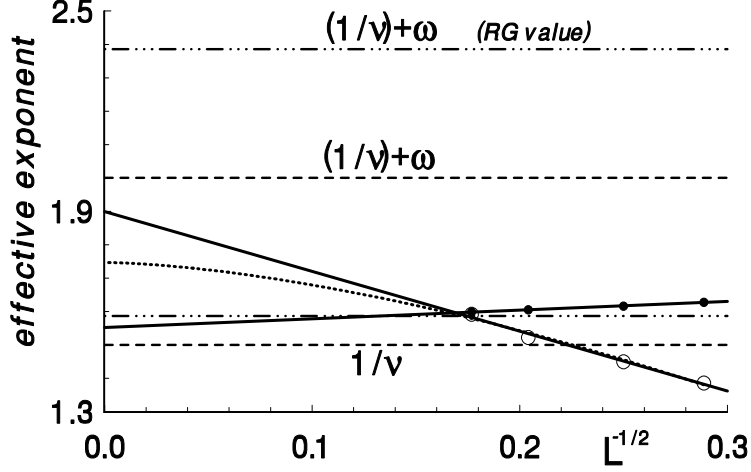


Figure 6: Effective critical exponents for the real (empty circles) and the imaginary (solid circles) part of complex partition-function-zeros of 3D Ising model depending on  $L^{-1/2}$ , where  $L$  is the linear size of the system. Solid lines show the linear least-squares fits. The asymptotic values from our theory are indicated by horizontal dashed lines, whereas those of the RG theory – by dot-dot-dashed lines. A selfconsistent extrapolation within the RG theory corresponds to the tiny dashed line.

conditions [22, 23]. The latter means that the critical behavior of real and imaginary parts of  $u_1^0 - u_c$  essentially differ from each other, i. e.,  $Re(u_1^0 - u_c) \propto L^{-(1/\nu)-\omega}$  and  $Im(u_1^0) \propto L^{-1/\nu}$  (where, in this case of  $d = 2$ ,  $\nu = \omega = 1$ ) at  $L \rightarrow \infty$ . The MC data of [9], in fact, provide a good evidence that the same is true in three dimensions.

Based on MC data for the partition function zeros in 3D Ising model, the authors of Ref. [9] have searched the way how to confirm the already known estimates for  $\nu$ . Their treatment, however, is rather doubtful. First, let us mention that, in contradiction to the definition in the paper,  $u_1^0$  values listed in Tab. I of [9] are not equal to  $e^{-\beta_1^0}$  (they look like  $e^{-4\beta_1^0}$ ). Second, the fit to a theoretical ansatz for  $|u_1^0(L) - u_c|$ , Eq. (6) in [9], is unsatisfactory. This ansatz contains a mysterious parameter  $a_3$ . If we compare Eqs. (5) and (6) in [9], then we see immediately that  $a_3 \equiv (1/\nu) + \omega$ . At the same time, the obtained estimate for  $a_3$ , i. e.  $a_3 = 4.861(84)$ , is completely inconsistent with the values of  $(1/\nu) + \omega$ , about 2.34, which follow from authors own considerations. Our prediction, consistent with the correction-to-scaling analysis in Sec. 2 (and with  $\ell = 4$  in (2) to coincide with the known exact result at  $d = 2$ ), is  $\nu = 2/3$  and  $\omega = 1/2$ , i. e.,  $(1/\nu) + \omega = 2$ .

To obtain a more complete picture, we have considered separately the real part and the imaginary part of  $u_1^0 - u_c$ . We have calculated  $u_1^0$  from  $\beta_1^0$  data listed in Tab. I of [9] and have estimated the effective critical exponents  $y'_{eff}(L)$  and  $y''_{eff}(L)$ , separately for  $Re(u_1^0 - u_c)$  and  $Im(u_1^0)$ , by fitting these quantities to an ansatz  $const \cdot L^{-y'_{eff}}$  and  $const \cdot L^{-y''_{eff}}$ , respectively, at sizes  $L$  and  $L/2$ . The value of  $u_c$  consistent with the estimation of the critical coupling in [27],  $\beta_c \simeq 0.2216545$ , has been used. The results are shown in Fig. 6. As we see,  $y'_{eff}$  (empty circles) claims to increase above  $y''_{eff}$  (solid circles) when  $L$  increases. This is a good numerical evidence that, like in the two-dimensional case, the asymptotic values are

$y' = \lim_{L \rightarrow \infty} y'_{eff}(L) = (1/\nu) + \omega$  and  $y'' = \lim_{L \rightarrow \infty} y''_{eff}(L) = 1/\nu$ . According to our theory, the actual plots in the  $L^{-1/2}$  scale are linear at  $L \rightarrow \infty$ , as consistent with the expansion in terms of  $L^{-\omega}$ . The linear least-squares fits are shown by solid lines. The zero intercepts 1.552 and 1.899 are in approximate agreement with our theoretical values 1.5 and 2 indicated by horizontal dashed lines. The relatively small discrepancy, presumably, is due to the extrapolation errors and inaccuracy in the simulated data. The result for  $y'$  is affected by the error in  $\beta_c$  value. However, this effect is negligibly small. Assuming a less accurate value  $\beta_c = 0.221659$ , consistent with the estimations in [32, 30], we obtain  $y' = 1.914$ .

The behavior of  $y'_{eff}$  is rather inconsistent with the RG predictions. On the one hand,  $y'_{eff}$  claims to increase above  $y''_{eff}$  and also well above the RG value of  $1/\nu$  (the lower dot-dot-dashed line at 1.586), and, on the other hand, the extrapolation yields  $y'$  value (1.899) which is remarkably smaller than  $(1/\nu) + \omega \simeq 2.385$  (the upper dot-dot-dashed line) predicted by the RG theory. For selfconsistency, we should use the linear extrapolation in the scale of  $L^{-\omega}$  with  $\omega = 0.799$  (the RG value). However, this extrapolation (tiny dashed line in Fig. 6), yielding  $y' \simeq 1.747$ , does not solve the problem in favour of the RG theory.

The data points of  $y'_{eff}$  look (and are expected to be) less accurate than those of  $y''_{eff}$ , since  $Re(u_1^0 - u_c)$  has a very small value. The  $y''_{eff}$  data do not look scattered, therefore they allow a refined analysis with account for nonlinear corrections. To obtain stable results, we have included the data for smaller lattice sizes  $L = 3$  and  $L = 4$  given in [24]. In principle, we can use rather arbitrary analytical function  $\phi(\beta)$  to evaluate the effective critical exponent

$$y''_{eff}(L) = \ln \left[ Im \phi \left( \beta_1^0(L/2) \right) / Im \phi \left( \beta_1^0(L) \right) \right] / \ln 2$$

and estimate its asymptotic value  $y''$ . For an optimal choice, however,  $y''_{eff}(L)$  vs  $L^{-\omega}$  plot should be as far as possible linear to minimize the extrapolation error. In this aspect, our choice  $\phi = \exp(-\beta)$  is preferable to  $\phi = \exp(-4\beta)$  used in [24]. We have tested also another possibility, i. e.  $\phi = \sinh(2\beta)$ , which appears as a natural parameter in the case of 2D Ising model. The shape of the  $y''_{eff}(L)$  plot can be satisfactory well approximated by a third-order, but not by a second-order, polynomial in  $L^{-1/2}$ , as it can be well seen when analyzing the local slope of this curve. The corresponding four parameter least-squares fits are shown in Fig. 7. They yield  $y'' \simeq 1.473$  in the case of  $\phi = \exp(-\beta)$  (long-dashed line) and  $y'' \simeq 1.518$  at  $\phi = \sinh(2\beta)$  (solid line). It is evident from Fig. 7 that in the latter case we have slightly better linearity of the fit, therefore  $1/\nu \simeq 1.518$  is our best estimate of the critical exponent  $1/\nu$  from the actual MC data. Thus, while the row estimation provided the value  $y'' = 1/\nu \simeq 1.552$  which is closer to the RG prediction  $1/\nu \simeq 1.586$  (horizontal dot-dot-dashed line), the refined analysis reveals remarkably better agreement with our (exact) value  $1/\nu = 1.5$  (horizontal dashed line).

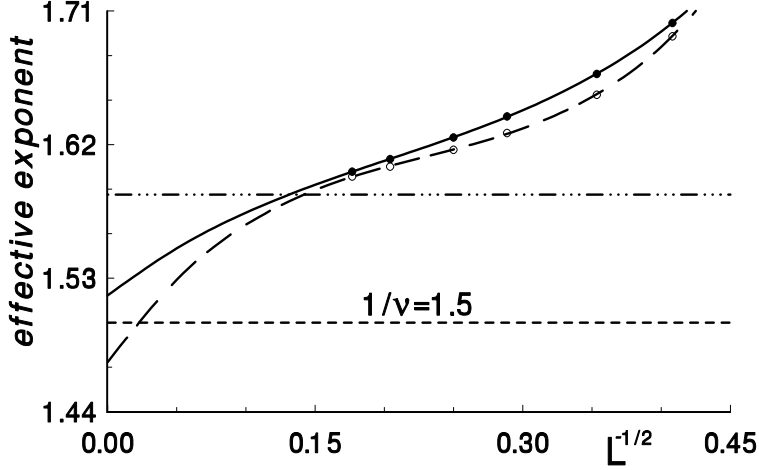


Figure 7: Effective critical exponent  $y''_{eff}(L)$  for the imaginary part of the complex partition-function-zeros as a function of  $L^{-1/2}$ , where  $L$  is the linear size of the system. The empty circles correspond to  $\phi = \exp(-\beta)$ , whereas the solid circles to  $\phi = \sinh(2\beta)$ . The corresponding least-squares fits  $y''_{eff}(L) = 1.4734 + 1.3321L^{-1/2} - 4.7587L^{-1} + 6.8894L^{-3/2}$  and  $y''_{eff}(L) = 1.5184 + 0.7271L^{-1/2} - 2.0309L^{-1} + 3.3095L^{-3/2}$  are shown by long-dashed line and solid line, respectively. Our asymptotic value  $y'' = 1/\nu = 1.5$  is indicated by horizontal dashed line, whereas that of the RG theory (1.586) – by dot-dot-dashed line.

## 6 $\lambda\varphi^4$ model and its crossover to Ising model

Here we discuss a  $\varphi^4$  model on a three-dimensional cubic lattice. The Hamiltonian of this model, further called  $\lambda\varphi^4$  model, is given by

$$H/T = \sum_{\mathbf{x}} \left\{ -2\kappa \sum_{\mu} \varphi_{\mathbf{x}} \varphi_{\mathbf{x}+\hat{\mu}} + \varphi_{\mathbf{x}}^2 + \lambda (\varphi_{\mathbf{x}}^2 - 1)^2 \right\}, \quad (41)$$

where the summation runs over all lattice sites,  $T$  is the temperature,  $\varphi_{\mathbf{x}} \in ]-\infty; +\infty[$  is the scalar order parameter at the site with coordinate  $\mathbf{x}$ ,  $\hat{\mu}$  is a unit vector in the  $\mu$ -th direction,  $\kappa$  and  $\lambda$  are coupling constants. Obviously, the standard 3D Ising model is recovered in the limit  $\lambda \rightarrow \infty$  where  $\varphi_{\mathbf{x}}^2$  fluctuations are suppressed so that, for a relevant configuration,  $\varphi_{\mathbf{x}}^2 \simeq 1$  or  $\varphi_{\mathbf{x}} \simeq \pm 1$  holds. The MC data for the Binder cumulant in this  $\lambda\varphi^4$  model have been interpreted in accordance with the  $\epsilon$ -expansion and a perfect agreement with the conventional RG values of critical exponents has been reported in [25]. According to the definition in [25], the Binder cumulant  $U$  is given by

$$U = \frac{\langle m^4 \rangle}{\langle m^2 \rangle^2}, \quad (42)$$

where  $m = L^{-3} \sum_{\mathbf{x}} \varphi_{\mathbf{x}}$  is the magnetization and  $L$  is the linear size of the system. Based on the  $\epsilon$ -expansion, it has been suggested in [25] that, in the thermodynamic limit  $L \rightarrow \infty$ , the value of the Binder cumulant at the critical point  $\kappa = \kappa_c(\lambda)$  and, equally, at a fixed ratio  $Z_a/Z_p = 0.5425$  (the precise value is not important) of

partition functions with periodic and antiperiodic boundary conditions is a universal constant  $U^*$  independent on  $\lambda$ . We suppose that the latter statement is true, but not due to the  $\epsilon$ -expansion. It is a consequence of some general argument of the RG theory: on the one hand,  $U$  is invariant under the RG transformation and, on the other hand, an unique fixed point (not necessarily the Wilson–Fisher fixed point) exists in the case of an infinite system, so that  $U \equiv U^*$  holds at  $L \rightarrow \infty$  and  $\kappa = \kappa_c(\lambda)$  where  $U^*$  is the fixed–point value of  $U$ . The above conclusion remains true if we allow that the fixed point is defined not uniquely in the sense that it contains some irrelevant degree(s) of freedom (like  $c^*$  and  $\Lambda$  in the perturbative RG theory discussed in Sec. 2 of [5]) not changing  $U$ . The numerical results in [27] confirm the idea that  $\lim_{L \rightarrow \infty} U(L) = U^*$  holds at criticality, where  $U^*$  is a universal constant independent on the specific microscopic structure of the Hamiltonian.

## 7 Estimation of the correction exponent $\omega$

Based on the idea that  $U^*$  is constant for a given universality class, here we estimate the correction–to–scaling exponent  $\omega$ . According to Sec. 2, corrections to finite–size scaling for the magnetization of the actual 3D Ising and  $\lambda\varphi^4$  models are represented by an expansion in terms of  $L^{-\omega}$  where  $\omega = 1/2$ . One expects that the magnetization (Binder) cumulant (42) has the same singular structure. Since  $\lim_{L \rightarrow \infty} U(L, \lambda) \equiv U^*$  holds at a fixed ratio  $Z_a/Z_p$ , a suitable ansatz for estimation of  $\omega$  is [25]

$$U(L, \lambda_1) - U(L, \lambda_2) \simeq \text{const} \cdot L^{-\omega} \quad \text{at} \quad Z_a/Z_p = 0.5425, \quad (43)$$

which is valid for any two different nonzero values  $\lambda_1$  and  $\lambda_2$  of the coupling constant  $\lambda$ . The data for  $\Delta U(L) = U(L, 0.8) - U(L, 1.5)$  can be read from Fig. 1 in [25] (after a proper magnification) without an essential loss of the numerical accuracy, i. e., within the shown error bars. Doing so, we have evaluated the effective exponent

$$\omega_{eff}(L) = \ln [\Delta U(L/2)/\Delta U(L)] / \ln 2, \quad (44)$$

i. e.,  $\omega_{eff}(12) \simeq 0.899$ ,  $\omega_{eff}(16) \simeq 0.855$ , and  $\omega_{eff}(24) \simeq 0.775$ . These values are shown in Fig. 8 by crosses. Such an estimation, however, can be remarkably influenced by the random scattering of the simulated data points, particularly, at larger sizes where  $\Delta U(L)$  becomes small. This effect can be diminished if the values of  $\Delta U(L)$  are read from a suitable smoothened curve. We have found that  $\Delta U(L)$  within  $L \in [7; 24]$  can be well approximated by a second–order polinomial in  $L^{-1/2}$ . The corresponding refined values  $\omega_{eff}(16) \simeq 0.8573$  and  $\omega_{eff}(24) \simeq 0.7956$  read from this curve are depicted in Fig. 8 by empty circles. These values are similar to those obtained by a direct calculation from the original data points (crosses).

In such a way, we see from Fig. 8 that the effective exponent  $\omega_{eff}(L)$  decreases remarkably with increasing of  $L$ . According to GFD theory,  $\omega_{eff}(L)$  is a linear function of  $L^{-1/2}$  at  $L \rightarrow \infty$ , as consistent with the expansion in terms of  $L^{-\omega}$  where  $\omega = 0.5$ . More data points, including larger sizes  $L$ , are necessary for a reliable estimation of the asymptotic exponent  $\omega = \lim_{L \rightarrow \infty} \omega_{eff}(L)$ . Nevertheless, already a row linear extrapolation in the scale of  $L^{-1/2}$  with the existing data points yields the result  $\omega \approx 0.547$  which is reasonably close to the exact value 0.5 (horizontal dashed line in Fig. 8) found within the GFD theory. The corresponding least–squares

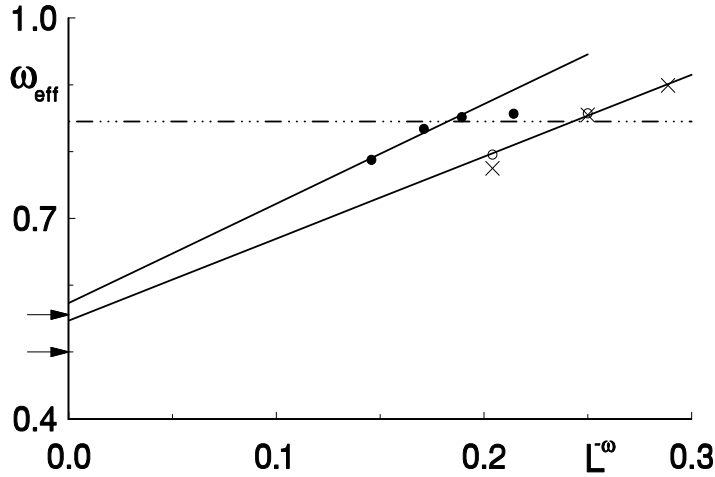


Figure 8: Effective correction-to-scaling exponent  $\omega_{eff}(L)$  in the  $O(n)$ -symmetric  $\lambda\varphi^4$  model with  $n = 1$  (empty circles and crosses) and  $O(2)$ -symmetric  $dd - XY$  model (solid circles) depending on the system size  $L$ . The linear least-squares fits give row estimates of the asymptotic  $\omega$  values 0.547 and 0.573, at  $n = 1$  and 2, respectively. The corresponding theoretical values of the GFD theory  $1/2$  and  $5/9$  (used in the  $L^{-\omega}$  scale of the horizontal axis) are indicated by arrows. The dot-dot-dashed line shows the value 0.845(10) proposed in [25] for the 3D Ising universality class ( $n = 1$ ).

fit with circles (at  $L = 24, 16$ ) and cross (at  $L = 12$ ) is shown in Fig. 8 by a straight solid line. It is evident from Fig. 8 that the final result  $\omega = 0.845(10)$  (horizontal dot-dot-dashed line) reported in [25] represents some average effective exponent for the interval  $L \in [6; 24]$ . It has been claimed in [25] that the estimates for  $\omega$  (cf. Tab. 2 in [25]) are rather stable with respect to a variation of  $L_{min}$ , where  $L_{min}$  is the minimal lattice size used in the fit. Unfortunately, the analysis has been made in an obscure fashion, i. e., giving no original data, so that we cannot check the correctness of this claim. Besides, the estimates in Tab. 2 of [25] has been made by using an ansatz

$$U(L, \lambda) = U^* + c_1(\lambda)L^{-\omega} \quad \text{at} \quad Z_a/Z_p = 0.5425, \quad (45)$$

which is worse than (43). Namely, (43) and (45) are approximations of the same order, but (45) contains an additional parameter  $U^*$  which is not known precisely. The results of an analysis with the ansatz (43), reflected in Tab. 5 of [25], are not convincing, since only very small values of  $L_{min}$  (up to  $L_{min} = 6$ ) have been considered.

In any case, we prefer to rely on that information we can check, and it shows that the claim in [25] that  $\omega = 0.845(10)$  holds with  $\pm 0.01$  accuracy cannot be correct, since  $\omega_{eff}(L)$  is varied in the first decimal place.

We have made a similar estimation of  $\omega$  for the dynamically diluted  $O(2)$ -symmetric ( $n = 2$ )  $XY$  ( $dd - XY$ ) model simulated in [26] ( $n = 2$ ). In the case of the  $dd - XY$  model, parameter  $D$  (cf. Eq.(6) in [26]) plays the role of  $\lambda$  in (43). The data for the Binder cumulant in Fig. 1 of [26] look rather accurate, i. e., not scattered. This enables us to estimate  $\omega_{eff}$  just from the data at  $D = 1.03$  and  $D = \infty$  ( $XY$

model). The resulting values of  $\omega_{eff}$  are depicted in Fig. 8 by solid circles. The scale of  $L^{-\omega}$  is used, where  $\omega = 5/9$  is our theoretical value of the correction-to-scaling exponent at  $n = 2$  consistent with the general hypothesis proposed in Sec. 2. As we see, the solid circles can be well located on a smooth line which, however, is remarkably curved at smaller sizes. Due to the latter reason, we have used only the last three points (the largest sizes) for the linear fit (solid line) resulting in an estimate  $\omega \approx 0.573$  which comes close to our theoretical value  $\omega = 5/9 = 0.555\dots$

In summary, the extrapolated  $\omega$  values (Fig. 8) in both cases  $n = 1$  and  $2$  are reasonably close to our theoretical values  $1/2$  and  $5/9$  indicated by arrows. Only a small systematic deviation is observed. This, likely, is due to the error of linear extrapolation: the  $\omega_{eff}(L)$  plots have a tendency to curve down slightly. The conventional (RG) estimate  $\omega \approx 0.8$  more or less corresponds to effective exponents for currently simulated finite system sizes, but not to the asymptotic exponents.

## 8 Fitting the susceptibility data at criticality

In this section we discuss some fits of MC data at criticality. According to the finite-size scaling theory, the susceptibility  $\chi$  near the critical point is represented by an expansion

$$\chi = L^{2-\eta} \left( g_0(L/\xi) + \sum_{l \geq 1} L^{-\omega_l} g_l(L/\xi) \right), \quad (46)$$

where  $g_l(L/\xi)$  are the scaling functions,  $\xi$  is the correlation length of an infinite system,  $\eta$  is the critical exponent related to the  $k^{-2+\eta}$  divergence of the correlation function in the wave vector space at criticality, and  $\omega_l$  are correction-to-scaling exponents,  $\omega_1 \equiv \omega$  being the leading correction exponent. The correlation length diverges like  $\xi \propto t^{-\nu}$  at  $t \rightarrow 0$ , where  $t = 1 - \beta/\beta_c$  is the reduced temperature. Thus, for large  $L$ , in close vicinity of the critical point where  $tL^{1/\nu} \ll 1$  holds Eq. (46) can be written as

$$\chi = a L^{2-\eta} \left( 1 + \sum_{l \geq 1} b_l L^{-\omega_l} + \delta(t, L) \right), \quad (47)$$

where  $a = g_0(0)$  and  $b_l = g_l(0)/g_0(0)$  are the amplitudes, and  $\delta(t, L)$  is a correction term which takes into account the deviation from criticality. In the first approximation it reads

$$\delta(t, L) \simeq c \cdot tL^{1/\nu}, \quad (48)$$

where  $c$  is a constant.

We start our analysis with the standard 3D Ising model with the Hamiltonian

$$H/T = -\beta \sum_{\langle ij \rangle} \sigma_i \sigma_j. \quad (49)$$

The critical point of this model has been found in [27] to be  $\beta_c \simeq 0.2216545$ . We have made our own tests with the data of [27], and have obtained the same value within the uncertainty of  $\pm 10^{-7}$ . From the maximal values of the derivative  $\partial \ln \langle m^2 \rangle / \partial \beta \equiv \partial \ln \chi / \partial \beta$  evaluated in [30] we conclude that the shift of  $\beta$  by  $10^{-7}$  produces the variation of  $\ln \chi$  at  $L = 96$  near  $\beta = \beta_c$ , which does not exceed  $4.7 \cdot 10^{-4}$  in magnitude.

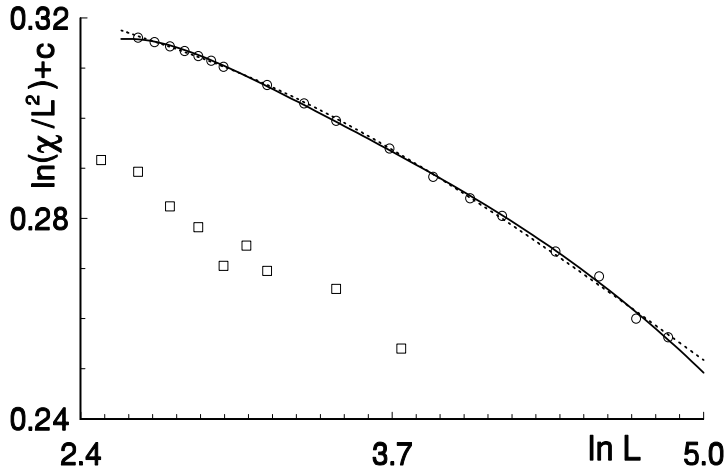


Figure 9: The fits of  $\ln(\chi/L^2)$  data at criticality (ansatz (47)) shifted by a constant  $c$ . Solid circles represent the MC data for 3D Ising model [27] at  $\beta = 0.2216545$  ( $c = 0$ ). The fits with our (GFD) exponents ( $\ln a = 1.065289, b_1 = -2.72056, b_2 = 8.18636, b_3 = -10.49614$ ) and with those of [25, 28] ( $\ln a = 0.430933, b_1 = 0.05850, b_2 = -7.74767, b_3 = 12.42890$ ) are shown by solid and tiny-dashed lines, respectively. The empty boxes are MC data for 3-component 3D XY model [29], shifted by  $c = 0.85$ .

The latter means that, with a good enough accuracy, we may assume that  $\beta_c$  is just 0.2216545 when fitting the susceptibility data at criticality within  $L \in [4; 128]$ . Here we mean the MC data given in Tab. 25 of [27]. We have made and compared several fits of these data to ansatz (47) with  $\delta(t, L) = 0$  (more precisely, to the corresponding formula for  $\ln \chi$ ) for two different sets of the critical exponents, i. e., our (GFD) and that proposed in [25]. The fits made with our exponents systematically improve relative to those made with the exponents of [25], as the system sizes grow and the approximation order increases. The necessity to include several correction terms is dictated by the fact that corrections to scaling are rather strong. According to the least-squares criterion, the fit with our exponents  $\eta = 1/8$  and  $\omega_l = l/2$  becomes better than that provided by the more conventional exponents  $\eta = 0.0358(4)$ ,  $\omega_1 = 0.845(1)$ ,  $\omega_2 = 2\omega_1$ , and  $\omega_3 = 2$  [25] starting with  $L_{min} = 28$  (i. e.,  $L \in [L_{min}; 128]$ ), if two correction terms ( $l = 1, 2$ ) are included. In the case of three correction terms it occurs already at  $L_{min} = 11$ . The four-parameter ( $a, b_1, b_2, b_3$ ) fits to MC data (empty circles) within  $L \in [14; 128]$  are shown in Fig. 9. The fit with our exponents (upper solid line) is relatively better at larger sizes. However, both fits (upper solid and dashed lines) look, in fact, quite similar, so that we cannot make unambiguous conclusions herefrom.

For comparison, we have shown in Fig. 9 also the MC data for 3D XY model [29], where the order parameter is 3-component vector with only two interacting components. As we see, the actual MC data (empty boxes) at  $\beta_c$  evaluated approximately  $\beta_c \simeq 0.6444$  [29] are rather scattered and, therefore, unsuitable for a refined analysis. Nevertheless, this is a typical situation where authors of such data make a very "accurate" and "convincing" estimation  $\gamma/\nu = 1.9696(37)$  or  $\eta = 0.0304(37)$  making a simple linear fit. However, the refined analysis given above has shown that even

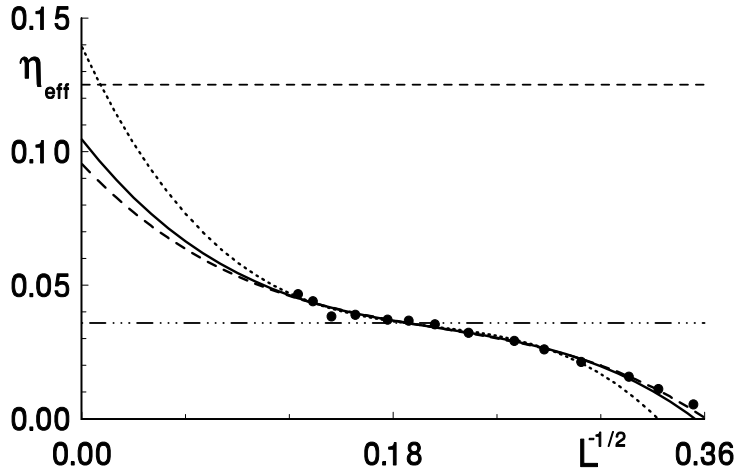


Figure 10: The effective critical exponent  $\eta_{eff}(L)$  (solid circles) obtained by fitting the susceptibility data of 3D Ising model at criticality ( $\beta = 0.2216545$ ) [27] within the interval  $[L; 2L]$ . The least-squares approximations obtained by fitting the  $\eta_{eff}(L)$  data within  $[L_{min}; 64]$  to a third-order polynomial in  $L^{-1/2}$  are shown by dashed ( $L_{min} = 9$ ), solid ( $L_{min} = 10$ ), and tiny-dashed ( $L_{min} = 12$ ) lines. The asymptotic value  $\eta = 1/8$  of the GFD theory is indicated by a horizontal dashed line. The dot-dot-dashed line represents the  $\eta$  value 0.0358 proposed in [25].

in the case of 3D Ising model, where the data are incompatibly more accurate, it is not so easy to distinguish between  $\eta = 0.0358$  and  $\eta = 1/8$ . Moreover, a refined analysis prefer the second value which is much larger than those usually provided by linear fits at typical system sizes  $L \leq 48$ . This is particularly well seen in Fig. 10, where the effective critical exponent  $\eta_{eff}(L)$  of the 3D Ising model, estimated via the linear fit within  $[L; 2L]$ , is depicted by solid circles. As we see,  $\eta_{eff}(L)$  tends to increase well above the conventional value 0.0358 (horizontal dot-dot-dashed line). The shape of the  $\eta_{eff}(L)$  plot is satisfactory well reproduced by a third-order polynomial in the actual scale of  $L^{-1/2}$ . Three such kind of least-squares approximations (at  $L_{min} = 9, 10, 12$ ) are shown in Fig. 10. These fits do not provide very accurate and stable asymptotic values of  $\eta$ . Nevertheless, they are more or less in agreement with our theoretical prediction  $\eta = 1/8$  (horizontal dashed line). Besides, the values of  $\eta_{eff}$  are affected by the error in  $\beta_c$  (about  $10^{-7}$ ) only slightly, i. e., by an amount not exceeding 0.001.

## 9 A test for 3D Ising model with "improved" action

Here we discuss some estimations of the critical exponents from the susceptibility data of 3D Ising model, reported in [27], with the so called "improved" action (i. e.,  $H/T$ ). One of the problems with the standard 3D Ising model is that corrections to scaling are strong. It has been proposed in [27] to solve this problem by considering a modified (spin-1) Ising model with the Hamiltonian

$$H/T = -\beta \sum_{\langle ij \rangle} \sigma_i \sigma_j + D \sum_i \sigma_i^2, \quad (50)$$



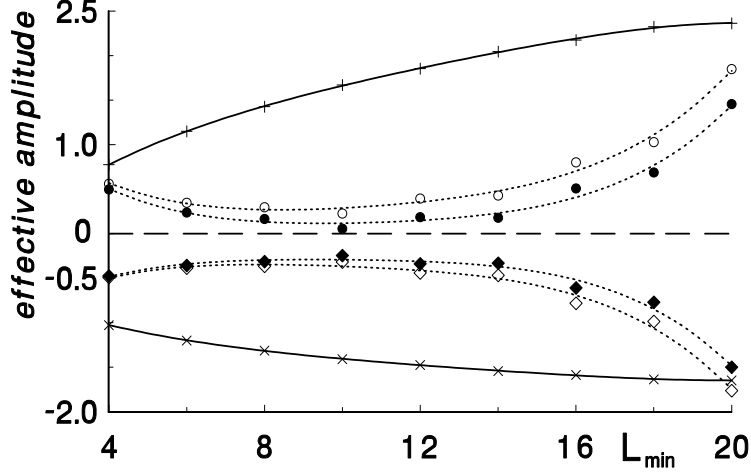


Figure 11: The effective amplitudes  $10b_1$  (circles) and  $b_2$  (rhombs) in (47) estimated at fixed exponents  $\eta = 0.0358$ ,  $\omega_1 = 0.845$ ,  $\omega_2 = 2\omega_1$ , and  $\nu = 0.6296$  by fitting the MC data within  $L \in [L_{min}; 56]$ . Filled symbols correspond to  $\delta(t, L) = 0$ , empty symbols – to  $\delta(t, L) = 10^{-6}L^{1/\nu}$ . The effective amplitudes  $b_1$  and  $b_2$  estimated with the critical exponents of our GFD theory ( $\eta = 1/8$ ,  $\omega_l = l/2$ ) at  $\delta(t, L) = 0$  are shown by "x" and "+", respectively. Lines represent the least-squares approximations by a fourth-order polynomial in  $L$ .

where the spin  $\sigma_i$  takes the values  $0, \pm 1$ , with two coupling constants  $\beta$  and  $D$  adjusted in such a way that the leading correction to finite-size scaling vanishes for all relevant physical quantities (magnetization cumulant, energy per site, susceptibility, etc.) and their derivatives. Moreover, according to the claims in [27] (see the conclusions in [27]), the ratios of the leading and subleading corrections are universal, so that not only the leading but all (!) corrections should vanish simultaneously.

We have checked the correctness of these claims as described below. We have fitted the corresponding to (47) expression for  $\ln \chi$  to the susceptibility data of the "improved" 3D Ising model (50) with  $(\beta, D) = (0.383245, 0.624235)$  (this is an approximation of the critical point) given in [27] (Tab. 26). By fixing the exponents, the least-squares fit within  $L \in [L_{min}; 56]$  (here  $L = 56$  is the maximal size available in Tab. 26 of [27]), including the leading and the subleading correction to scaling, provides the effective amplitudes  $a$ ,  $b_1$ , and  $b_2$  depending on  $L_{min}$ . We have made a test with the critical exponents  $\eta = 0.0358(4)$ ,  $\omega = 0.845(10)$ , and  $\nu = 0.6296(3)$  proposed in [25]. These values are close to those of the usual RG expansions [28], but, as claimed in [25], they are more accurate. According to [25], the asymptotic expansion contains corrections like  $L^{-n\omega}$  and  $L^{-2n}$ , where  $n = 1, 2, 3, \dots$ . Thus we have  $\omega_1 = \omega$  and  $\omega_2 = 2\omega$ . The resulting amplitudes  $10b_1(L_{min})$  and  $b_2(L_{min})$  are shown in Fig. 11 by circles and rhombs, respectively. We have depicted by filled symbols the results of the fitting with  $\delta(t, L) = 0$ , assuming that the critical coupling  $\beta_c = 0.383245$  has been estimated in [25] with a high enough (6 digit) accuracy. The data points quite well fit smooth (tiny dashed) lines within  $L_{min} \in [4; 20]$ , which means that the statistical errors are reasonably small. If the exponents used in the fit are correct and corrections to scaling are small indeed, then the convergence of the effective amplitudes to some small values is expected with increasing of  $L_{min}$ .

However, as we see from Fig. 11, the effective amplitudes tend to increase in magnitude acceleratedly as  $L_{min}$  exceeds 14. A small inaccuracy in  $\beta_c$  value can be compensated by the term  $\delta(t, L) \simeq c^* L^{1/\nu}$  in (47), where  $c^* = ct$  (cf. Eq. (48)). The results of fitting with  $c^* = 10^{-6}$  are shown in Fig. 11 by empty symbols. As we see, the expected inaccuracy in  $\beta_c$  of order  $10^{-6}$  does not change the qualitative picture. The increase of the effective amplitudes indicates that either the exponents are false, or the asymptotic amplitudes are not small (or both). This is our argument that the claims in [27] about very accurate critical exponents, extracted from the 3D Ising model with "improved" action, are incorrect.

For comparison, we have shown in Fig. 11 also the effective amplitudes  $b_1(L_{min})$  and  $b_2(L_{min})$  (by "x" and "+", respectively) estimated with the critical exponents of our GFD theory (Sec. 2) ( $\eta = 1/8$ ,  $\omega_l = l/2$ ), assuming  $\delta(t, L) = 0$ . The effective amplitudes converge to some values with increasing of  $L_{min}$ . These, however, are not the true asymptotic values, since the maximal size of the system has been eliminated to  $L = 56$ .

## 10 A test for the standard 3D Ising model

A test with the effective amplitudes, as in Sec. 9, appears to be more sensitive tool as compared to the fits discussed in Sec. 8. Here we consider the standard 3D Ising model. We have fitted all data points in Tab. 25 of [27] within the interval of sizes  $[L; 8L]$  to the theoretical expression for  $\ln \chi$  (consistent with (47)) to evaluate the effective amplitudes  $a$  and  $b_l$  with  $l = 1, 2, 3$  depending on  $L$ . Exceptionally in the case if all the involved exponents are correct (exact) each effective amplitude can converge to a certain nonzero asymptotic value at  $L \rightarrow \infty$ . In other words, if one tries to compensate the inconsistency in the exponent by choosing appropriate amplitude, then the amplitude tends either to zero or infinity at  $L \rightarrow \infty$ .

We have shown in Fig. 12 the effective amplitudes  $\ln a(L)$  and  $b_l(L)$  in the case of our critical exponents  $\eta = 1/8$  and  $\omega_l = l/2$ . As we expected, the effective amplitudes converge to some nonzero values with increasing of  $L$ . This is a good numerical evidence that our critical exponents are true. The case with the exponents of [25]  $\eta = 0.0358(4)$ ,  $\omega_1 = 0.845(10)$ ,  $\omega_2 = 2\omega_1$ , and  $\omega_3 = 2$  is illustrated in Fig. 13. As we expected, the effective amplitudes of our four-parameter fit (solid symbols) tend to diverge with increasing of  $L$ , which shows that this set of critical exponents is false. One could object that, probably, the instability of the effective amplitudes is due to small errors in MC data. However, the amplitudes  $b_1(L)$  and  $b_2(L)$  of the more stable three-parameter fit ( $l = 1, 2$  in (47)) behave in a similar way (see empty symbols in Fig. 13). Moreover, the amplitude  $b_1(L)$  of the two-parameter fit, shown by crosses, increases almost linearly at large enough  $L$  instead of the expected (in a case of correct exponents) saturation like  $b_1(L) \simeq b_1 + const \cdot L^{-\omega}$ . As regards the convergence in Fig. 12 of the effective amplitudes at  $L \rightarrow \infty$ , it is possible only if both conditions are fulfilled, i. e., the exponents are correct and the MC data are accurate enough to ensure stable results. Thus, in any case, the analysis in Fig. 12 provides rather convincing evidence that our exponents are the true ones, which by itself rules out the possibility that those proposed in [25] could be correct. The results in Figs. 12 and 13 are affected insignificantly by a small inaccuracy of about  $10^{-7}$  in the estimated  $\beta_c$  value.

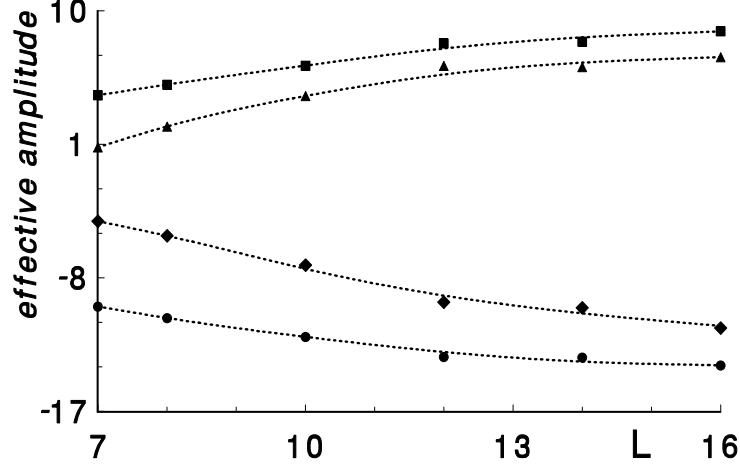


Figure 12: The effective amplitudes in Eq. (47)  $100(\ln a(L)-1)$  (triangles),  $5b_1(L)$  (circles),  $b_2(L)$  (squares), and  $b_3(L)$  (rhombs) evaluated by fitting the susceptibility data of 3D Ising model at criticality within the interval of sizes  $[L; 8L]$  with the critical exponents  $\eta = 1/8$  and  $\omega_l = l/2$  of the GFD theory.

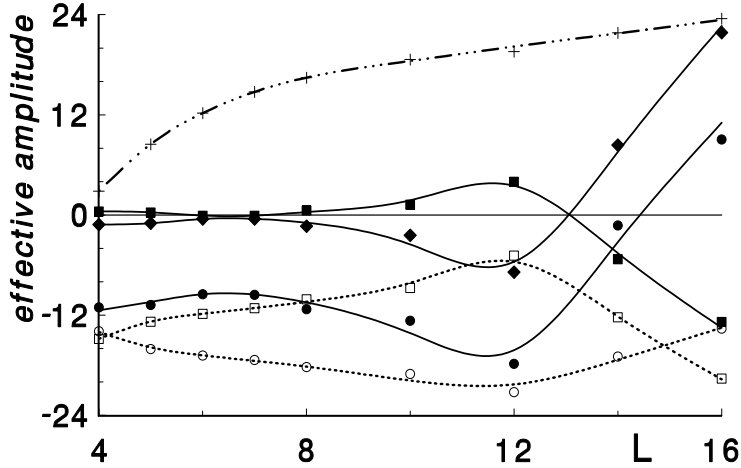


Figure 13: The effective amplitudes in Eq. (47) evaluated by fitting the susceptibility data of 3D Ising model at criticality within the interval of sizes  $[L; 8L]$  with the critical exponents  $\eta = 0.0358$ ,  $\omega_1 = 0.845$ ,  $\omega_2 = 2\omega_1$ , and  $\omega_3 = 2$  proposed in [25]. Solid symbols show the four-parameter fit:  $50b_1(L)$  (circles),  $b_2(L)$  (squares), and  $b_3(L)$  (rhombs); empty symbols show the three-parameter fit:  $100b_1(L)$  (circles) and  $27b_2(L)$  (squares); crosses represent the amplitude of the two-parameter fit, i. e., quantity  $190(b_l(L) + 0.34)$ .

## 11 Remarks about other numerical results

There exists a large number of numerical results in the published literature not discussed here and in [5]. A detailed review of these results is given in [31]. The cited there papers report results which disagree with the values of the critical exponents we have proposed. However, as regards the pure Monte Carlo study, we are quite confident that, just like in the actually discussed case of 3D Ising model, the increase of system sizes and/or use of higher-level approximations will lead to the conclusion that fits with our exponents are better than those with the conventional (RG) exponents. Particularly, a careful analysis of the effective exponents made in Secs. 5, 7, and 8 already has shown that the effective exponents deviate from the values predicted by the perturbative RG theory and converge more or less to those of the GFD theory at  $L \rightarrow \infty$ . Together with the analysis of the experiment with superfluid  $^4\text{He}$  [5], we have presented totally 5 independent evidences of such a behavior. Besides, an important prediction of exceptionally our theory regarding the corrections to scaling is confirmed by the exact-algorithm transfer matrix calculations in Sec. 4.3.

There exists some background for the conventional claims in the published literature that all the usual methods give consistent results which appear to be in a good agreement with the predictions of the perturbative RG theory. The perturbation expansions of the RG theory, as well as the techniques of high- and low-temperature series expansion are merely not rigorous extrapolation schemes which work not too close to criticality. As a result, these methods produce some pseudo or effective critical exponents which, however, often provide a good approximation just for the range of temperatures not too close to  $T_c$  (critical temperature) where these methods make sense and, therefore, agree with each other. According to the finite-size scaling theory,  $tL^{1/\nu}$  is a relevant scaling argument, so that not too small values of the reduced temperature  $t$  are related to not too large sizes  $L \sim t^{-\nu}$ . Therefore, one can understand that the MC results for finite systems often can be well matched to the conventional critical exponents proposed by high temperature (HT) and RG expansions. If, however, the level of MC analysis (i. e., the level of approximations used) is increased, then it turns out that the "conventional" critical exponents are not valid anymore, as it has been demonstrated in the current paper. It is because the "conventional" exponents are not the asymptotic exponents. Correct values of the asymptotic exponents have been found in [5] considering suitable theoretical limits instead of formal expansions in terms of  $\ln k$  (at criticality, where  $k$  is the wave vector magnitude) or  $\ln t$  (approaching criticality) which are meaningless at  $k \rightarrow 0$  and  $t \rightarrow 0$ . These formal expansions lie in the basis of the RG expansions for the critical exponents. One argue that  $\ln k$  diverges weakly, therefore the expansions in powers of  $\ln k$  can be treated. This is a nonsense: any term like  $k^{-\lambda}$  with  $\lambda < 0$  can be formally expanded in terms of  $\ln k$ , but therefore it does not become less divergent. Moreover, not only the powers of  $k$  but almost any function can be expanded in terms of  $\ln k$ , therefore it is impossible to decipher what is hidden behind such formal expansions in reality. This is a serious problem, since even an exponentially small correction (at  $k \rightarrow 0$ ) can give a nonvanishing contribution to such a formal expansion (see examples in Sec. 2 of [5]). The problem is not only formal: it has been proven in [5] that the assumption that the  $\epsilon$ -expansion works and provides

correct results at  $k \rightarrow 0$  leads to an obvious contradiction in mathematics (cf. Sec. 2 in [5]). This fact alone cannot be compensated even by an infinite number of numerical evidences supporting the "conventional" critical exponents coming from the RG expansions.

Our arguments, based on the current numerical analysis, are the following. First, the calculations by exact algorithms in Sec. 4.3 confirm our theoretical prediction, but not that of the perturbative RG theory. Second, we have proposed here a very sensitive method (i. e., a study of effective amplitudes) which allows to test the consistency of a given set of critical exponents with the MC data including several (in our case up to 3) corrections to scaling. We have applied this method to one of the recent and most accurate numerical data for the susceptibility in 3D Ising model, and have got a confirmation that our critical exponents are true. It would be not correct to doubt our results based on less sensitive methods and lower-level approximations.

We prefer to rely just on the data of pure MC simulations because of the following reasons. The so called Monte Carlo RG (MCRG) method is not free of assumptions related to approximate renormalization. We would like only to mention that the MCRG study in [33] of 3D Ising systems of the largest (to our knowledge) available in literature sizes, i. e. up to  $L = 256$ , has not revealed an excellent agreement with the usual predictions of the perturbative RG. In particular, an estimate  $\omega \approx 0.7$  has been obtained [33] which is smaller than the usual (perturbative) RG value  $\approx 0.8$ , but still is larger than the exact value 0.5 predicted by the GFD theory. The high-temperature series cannot give more precise results than those extracted from the recent most accurate MC data, including the actual data of [27], since these series diverge approaching the critical point. One approximates the divergent series by a ratio of two divergent series (Pade approximation), but it is never proven that such a method converges to the exact result. Besides, the comparison to our calculations in 2D Ising model via exact algorithms (Sec. 4) shows that the HT series analysis leads to misleading conclusions regarding such fine effects as corrections to scaling. These effects are relevant for 3D models. It is interesting to compare the MC and HT estimates of the critical point for the standard 3D Ising model, i. e.,  $\beta_c \simeq 0.2216545$  (MC) [27] and  $\beta_c = 0.221659 + 0.000002 / - 0.000005$  (HT) [32]. It is clear that the MC value is more accurate: if we look in [27], where the estimation procedure is well illustrated, we can see that  $\beta_c$  is definitely smaller than 0.221659, and the error seems to be much smaller than the difference between both estimates 0.0000045. As we have mentioned already, our independent tests suggest that the error of the actual MC value is about  $10^{-7}$ .

## 12 Conclusions

Summarizing the present work we conclude the following:

1. Critical exponents and corrections to scaling for different physical quantities have been discussed in framework of our [5] recently developed GFD (grouping of Feynman diagrams) theory (Sec. 2).
2. Calculation of the two-point correlation function of 2D Ising model at the critical point has been made numerically by exact transfer matrix algorithms

(Secs. 3 and 4). The results for finite lattices including up to 800 spins have shown the existence of a nontrivial correction to scaling with a very small amplitude and exponent about  $1/4$  in agreement with the prediction of our GFD theory. No correction with the conventionally predicted exponent  $4/3$  has been detected.

3. The recently published Monte Carlo data for several three-dimensional lattice models have been reanalyzed. This analysis in Secs. 5 to 8 has shown that the effective critical exponents deviate from the values predicted by the perturbative RG theory and converge towards those of the GFD theory at  $L \rightarrow \infty$ . The same behavior has been observed in the experiment with superfluid  $^4\text{He}$  discussed in [5]. Totally, these are five independent evidences of such a behavior, suggesting that the above examples are not occasional or exceptional, but reflect a general rule.
4. Different sets of critical exponents (one provided by GFD theory, another proposed in [25]) predicted for the 3D Ising model have been tested by analyzing the effective amplitudes (Sec. 9 and 10). While the usual fits of the susceptibility data do not allow to show convincingly which of the discussed here sets of the critical exponents is better, this method strongly suggests that the conventional critical exponents  $\eta = 0.0358(4)$  and  $\omega = 0.845(10)$  [25] are false, whereas our (GFD) values  $\eta = 1/8$  and  $\omega = 1/2$  are true.

## Acknowledgements

This work including numerical calculations of the 2D Ising model have been performed during my stay at the Graduiertenkolleg *Stark korrelierte Vielteilchensysteme* of the Physics Department, Rostock University, Germany.

## References

- [1] L. Onsager, Phys. Rev. **65** (1944) 117
- [2] D. Sornette, Critical Phenomena in Natural Sciences, Springer, Berlin, 2000
- [3] J. G. Brankov, D. M. Danchev, N. S. Tonchev, Theory of Critical Phenomena in Finite-Size Systems: Scaling and Quantum Effects, World Scientific, 2000
- [4] Rodney J. Baxter, Exactly Solved Models in Statistical Mechanics, Academic Press, London, 1989
- [5] J. Kaupužs, Ann. Phys. (Leipzig) **10** (2001) 299
- [6] N. Ito, M. Suzuki, Progress of Theoretical Physics, **77** (1987) 1391
- [7] N. Schultka, E. Manousakis, Phys. Rev. B **52** (1995) 7258
- [8] L. S. Goldner, G. Ahlers, Phys. Rev. B **45** (1992) 13129
- [9] N. A. Alves, J. R. Drugowich, U. H. E. Hansmann, J. Phys. A **33** (2000) 7489

- [10] K. G. Wilson, M. E. Fisher, Phys. Rev. Lett. **28** (1972) 240
- [11] Shang–Keng Ma, Modern Theory of Critical Phenomena, W.A. Benjamin, Inc., New York, 1976
- [12] J. Zinn–Justin, Quantum Field Theory and Critical Phenomena, Clarendon Press, Oxford, 1996
- [13] H. Chamati, Eur. Phys. J. B **24** (2001) 241
- [14] C. Holm, W. Janke, Phys. Rev. B **48** (1993) 936
- [15] H. G. Ballesteros, L. A. Fernandez, V. Martin–Mayor, A. M. Sudupe, Phys. Lett. B **387** (1996) 125
- [16] K. Huang, Statistical Mechanics, John Wiley & Sons, New York 1963
- [17] M. Barma, M. Fisher, Phys. Rev. Lett. **53** (1984) 1935
- [18] B. Nickel, J. Phys. A **33** (2000) 1693
- [19] A. Bednorz, J. Phys. A, **33** (2000) 5457
- [20] L. Landau, E. Lifshitz, Course of Theoretical Physics, Part 5: Statistical Physics, §141, Moscow, 1964
- [21] R. Brout, Phase Transitions, New York, 1965
- [22] W. Janke, R. Kenna, Phys. Rev. B **65** (2002) 064110
- [23] W. Janke, R. Kenna, Nucl. Phys. B (Proc. suppl.) **106–107** (2002) 929
- [24] N. A. Alves, B. A. Berg, R. Villanova, Phys. Rev. B **41** (1990) 383
- [25] M. Hasenbusch, J. Phys. A **32** (1999) 4851
- [26] E. Campostrini, M. Hasenbusch, A. Pelissetto, P. Rossi, E. Vicary, Phys. Rev. B **63** (2001) 214503
- [27] M. Hasenbusch, K. Pinn, S. Vinti, Phys. Rev. B **59** (1999) 11 471
- [28] R. Guida, J. Zinn–Justin, J. Phys. A **31** (1998) 8103
- [29] K. Nho, E. Manousakis, Phys. Rev. B **59** (1999) 11575
- [30] A. M. Ferrenberg, D. P. Landau, Phys. Rev. B **44** (1991) 5081
- [31] A. Pinossetti, E. Vicari, e–print cond–mat/0012164
- [32] Z. Salman, J. Adler, Int. J. Modern Physics C **9** (1998) 195
- [33] R. Gupta, P. Tamayo, Int. J. Mod. Phys. C **7** (1996) 305